FINAL REPORT

on

DOUBLE TIME LAG COMBUSTION INSTABILITY MODEL FOR BIPROPELLANT ROCKET ENGINES

by

CHANG KENG LIU
Principal Investigator

Prepared for

National Aeronautics and Space Administration
George C. Marshall Space Flight Center
Marshall Space Flight Center, Alabama 35812

September, 1973

BER Report No. 158-80

FINAL REPORT

on

DOUBLE TIME LAG COMBUSTION INSTABILITY MODEL FOR BIPROPELLANT ROCKET ENGINES

by

CHANG KENG LIU
Principal Investigator

Prepared for

National Aeronautics and Space Administration
George C. Marshall Space Flight Center
Marshall Space Flight Center, Alabama 35812

September, 1973

BER Report No. 158-80

DOUBLE TIME LAG COMBUSTION INSTABILITY MODEL FOR BIPROPELLANT ROCKET ENGINES

INTRODUCTION

Since it was first observed in the early 1940's, low frequency combustion instability or chugging in liquid rocket engines has been the subject of many analyses. Von Karman (1) was the first to propose that the phenomenon is due to a combustion time delay between the instant of propellant injection and subsequent conversion into combustion products. In 1950 Gunder and Friant (2) presented an analysis in which this combustion delay was the essential feature but also included the inertia of the liquid in the feed system. This was followed about one year later with an analysis by Summerfield (1) which also incorporated the combustion delay and feed system inertia. Gunder and Friant treated both monopropellant and bipropellant rocket systems with a common combustion delay for the latter case. Summerfield treated only the monopropellant case. In both of these analyses the authors showed that instability is not possible if the pressure drop across the injector is greater than one-half the chamber pressure. Crocco and Cheng (3) later refined the model for the monopropellant case by assuming a time varying combustion delay which for simplicity was correlated to chamber pressure. Their analysis considered feed system inertance and capacitance as well as resistance. Hurrell (4) introduced the concept of an injection velocity-dependent combustion delay and

its effect on the neutral stability boundaries. More recently Wenzel and Szuch (5) conducted an analysis of the bipropellant case by allowing different vaporization rates for the two propellants. However, feed system inertance and capacitance were not considered. An interesting conclusion from this work was that in some cases decreasing the ratio of the injection pressure drop to chamber pressure results in a transition from unstable to stable operation. This cannot be predicted from single combustion delay analyses.

All of these analyses have served to establish the current knowledge and understanding of low frequency combustion instability and have guided the prevention and/or elimination of the phenomenon in past rocket engine development work. However, in analyzing current high chamber pressure, bipropellant rocket engines with propellants possessing distinctly different vaporization rates (time lags), these analyses have certain shortcomings. First, the analysis of a bipropellant rocket engine with a monopropellant model applied individually to each propellant system yields questionable results because it neglects the influence of the other system on the overall stability. Second, the use of a bipropellant model with a common combustion delay to represent propellants with distinctly different vaporization rates is unrealistic. And third, in view of the fact that feed system inertance and capacitance play an important role along with injection pressure drop in determining the stability of the overall system, these factors should also be included in the model. It should be possible, at lease in some cases, to stabilize the combustion with less impact to the overall rocket system by optimizing these parameters rather than adjusting only the pressure drop. Reliance on an injection pressure drop greater than one-half the

chamber pressure to guarantee stability is unrealistic from both the standpoint of high pump discharge pressures that would be required for today's engines and from the results of the analysis of Wenzel and Szuch.

This report advances a bipropellant stability model in which feed system inertance and capacitance are treated along with injection pressure drop and distinctly different propellant time lags. The model is essentially an extension of Crocco's and Cheng's monopropellant model to the bipropellant case assuming that the feed system inertance and capacitance along with the resistance are located at the injector. The neutral stability boundaries are computed in terms of these parameters to demonstrate the interaction among them.

Combustion Chamber and Associated Equations

Crocco's ingenious derivation of the combustion chamber equation is based only on a limited number of fundamental assumptions and definitions. First, like Summerfield, he postulates that the chamber pressure p is a function of time t, even when the combustion process is a steady one. Next, he suggests that the rate of combustion processes in the chamber is a function of several variables, the two more prominent of which are pressure and temperature; the rest of the relevant variables are lumped into a single group, Z. Thus, without identifying the nature of the combustion process, he states neatly,

$$\text{Process Rate} = f(p,T,Z) = f(\bar{p},\bar{T},\bar{Z})\left[1 + p' \frac{\text{H.D.T.}}{f(\bar{p},\bar{T},\bar{Z})}\right] \qquad (1)$$

where the bars on the variables indicate the steady-state values of these variables, and $p' = p - \bar{p}$ is the small perturbation of the chamber pressure, and H.D.T. denotes the higher derivative terms, such as

$$\left(\frac{\partial f}{\partial p} + \frac{\partial f}{\partial T}\frac{dT}{dp} + \frac{\partial f}{\partial Z}\frac{dZ}{dp}\right)\Bigg|_{p=\bar{p},\ T=\bar{T},\ Z=\bar{Z}}.$$

In so doing, Crocco singles out the predominant effects of pressure on the process rate f, and disregards those of the others. As it will be shown later that, out of this perfectly general and vague definition of f, Crocco was able to lay the foundation for the formulation of the relationship between the burning and the injection rates of the propellant.

From the definition of f just introduced, it is easily obtained by transposition

$$n = \frac{p'(H.D.T.)}{f(\bar{p},\bar{T},\bar{Z})} = \frac{f(p,T,Z) - f(\bar{p},\bar{T},\bar{Z})}{f(\bar{p},\bar{T},\bar{Z})} \qquad (2)$$

where n is simply the percent change of process rate, with respect to the steady state process rate, due to a small perturbation in pressure, p'. Crocco and Cheng call this % change the interaction index. This index seems to reflect, to some degree, the design of combustion chamber.

The next innovation that Crocco introduced at the outset of his investigation in combustion instability is the concept of a time lag, τ_t, which is the total time elapsed between the instant when n = 0 and the instant when n = 1. To simplify the ensuing analyses, he assumes further that during a certain portion of this time lag, i.e. τ_i, the interaction index n is zero and during the rest, i.e. $\tau = \tau_t - \tau_i$, n = 1. Thus, τ_i is the insensitive part and τ is the sensitive part of the total time lag τ_t.

With these two quantities defined, the following statement concerning the energy E_a contained in a certain element of propellant as it transforms from liquid state into gaseous products of combustion can be made

$$\int_{t-\tau}^{t} f(t')\, dt' = E_a \qquad (3)$$

Note that the lower limit of the integral is the instant when the process rates begin to be affected by the combustion processes. Note, too, that this same level of energy E_a would have been reached also, if the processes of combustion had been steady. Thus, it is equally valid

$$\int_{t-\bar{\tau}}^{t} \bar{f}(t')\, dt' = E_a \qquad (4)$$

where the schematic variation of the rate function f with respect to the time lags τ and $\bar{\tau}$ are shown in Figure A.

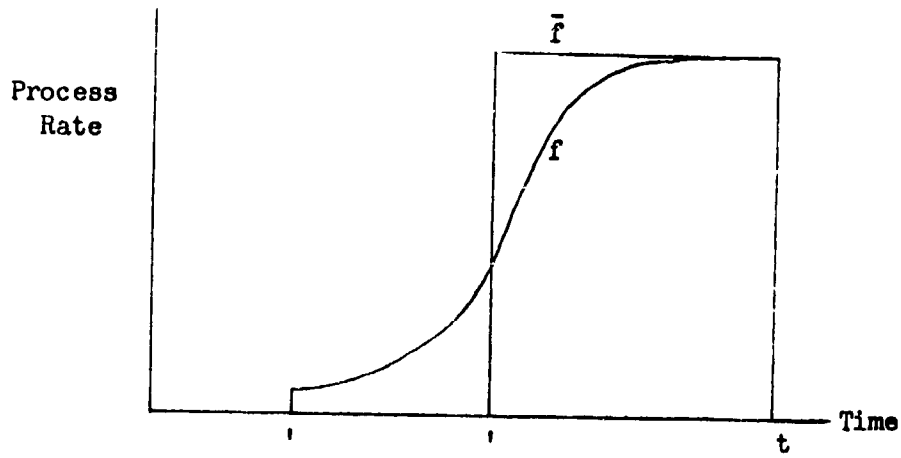

Fig. A

Observing the schematic variation of f(t), one may write

$$\int_{t-\tau}^{t-\bar{\tau}} f(t')\, dt' + \int_{t-\bar{\tau}}^{t} f(t')\, dt' = E_a = \int_{t-\bar{\tau}}^{t} \bar{f}(t')\, dt' \qquad (5)$$

The first integral on the left-hand side of (5) can be rewritten approximately,

$$\int_{t-\tau}^{t-\bar{\tau}} f(t')\, dt' \simeq [(t - \bar{\tau}) - (t - \tau)]\, \bar{f}(t-\bar{\tau}) = (\tau - \bar{\tau})\, \bar{f}(t - \bar{\tau}) \qquad (6)$$

Transposing,

$$t-\bar{\tau} = \frac{1}{\bar{f}(t-\bar{\tau})} \int_{t-\tau}^{t-\bar{\tau}} f(t') \, dt' \tag{7}$$

But, from (5),

$$\int_{t-\tau}^{t-\bar{\tau}} f(t') \, dt' = - \int_{t-\bar{\tau}}^{t} [f(t') - \bar{f}(t')] \, dt'$$

hence, (7) becomes

$$\tau-\bar{\tau} = - \int_{t-\bar{\tau}}^{t} \frac{f(t') - \bar{f}(t')}{f(t-\bar{\tau})} \, dt' \sim - \int_{t-\bar{\tau}}^{t} \frac{f(t') - \bar{f}(t')}{\bar{f}(t')} \, dt'$$

Using the definition of n from (2), we have

$$\tau-\bar{\tau} = - \frac{n}{\bar{p}} \int_{t-\bar{\tau}}^{t} p'(t') \, dt' \tag{8}$$

Differentiation with respect to t of $\tau-\bar{\tau}$ under the integral sign yields then

$$\frac{d\tau}{dt} = - \frac{n}{\bar{p}} [p'(t) - p'(t-\bar{\tau})] \tag{9}$$

This equation only portrays a part of the combustion chamber phenomenon.

The second part of the derivation of the chamber equation is concerned with the mass balance in the combustion chamber. It begins with the premise that the mass of propellant injected equals the mass burned at an instant τ_t later.

$$\delta\dot{m}_i(t) \, dt = \delta\dot{m}_b(t+\tau_t) \, (dt + d\tau) \tag{10}$$

where the subscripts i and b denote injection and burning, respectively. The time lag τ_t in (10) is approximately equal to and will be later

replaced by its counterpart $\bar{\tau}_t$ in the steady state process. Now let

$$t+\bar{\tau}_t = \tilde{T} \qquad \text{or} \qquad t=\tilde{T} - \bar{\tau}_t.$$

Eq. (10) becomes

$$\delta\dot{m}_i(\tilde{T}-\bar{\tau}_t)\ (d\tilde{T}-d\tau) = \delta\dot{m}_b(\tilde{T})\ d\tilde{T}$$

or

$$\delta\dot{m}_b(\tilde{T}) = \delta\dot{m}_i(\tilde{T}-\bar{\tau}_t)\ (1-\frac{d\tau}{d\tilde{T}})$$

Renaming $\tilde{T}$ as t. as the starting instant of the process is immaterial, we have

$$\delta\dot{m}_b(t) = \delta\dot{m}_i(t-\bar{\tau}_t)\ (1 - \frac{d\tau}{dt}) \tag{11}$$

Eq. (1) is now modified slightly, with the understanding that in a steady-state process $\delta\bar{\dot{m}}_i = \delta\bar{\dot{m}}_b$,

$$\delta\dot{m}_b(t) - \delta\bar{\dot{m}}_b = \delta\dot{m}_i(t-\bar{\tau}_t) - \delta\bar{\dot{m}}_i - \frac{d\tau}{dt}\ \delta\dot{m}_i(t-\bar{\tau}) \tag{12}$$

If the injection rate is constant, i.e. $\delta\dot{m}_i(t) = \delta\bar{\dot{m}}_i = \delta\bar{\dot{m}}_b$, it follows then

$$\delta\dot{m}_b(t) = \delta\bar{\dot{m}}_b\ (1 - \frac{d\tau}{dt}).$$

The next phase of investigation deals with the dynamics of the combustion chamber. For a non-steady process we can write

$$\dot{m}_p(t) = \dot{m}_e(t) + \frac{d}{dt}\ M_g(t) \tag{13}$$

where $\dot{m}_b(t)$ is the rate of generation of combustion products, $\dot{m}_e(t)$ is the rate of ejection of gases through the nozzle, and $M_g(t)$ is the mass of gases accumulated inside the chamber. Since $M_g(t)$ is proportional to the chamber pressure, the rate of accumulation of $M_g(t)$ is

$$\frac{d}{dt} M_g(t) = \bar{M}_g \frac{d}{dt} \left[\frac{p(t)}{\bar{p}}\right]$$

where $\bar{M}_g$ is the steady-state value of $M_g(t)$.

Considering the total amount of the combustion product from t = 0 to the current instant t = t, we have

$$\int_0^t \dot{m}_b(t')\, dt' = \int_0^{t-\tau_t} \dot{m}_i(t')\, dt' \tag{14}$$

Differentiation of (14) with respect to t gives

$$\dot{m}_b(t) = (1 - \frac{d\tau}{dt})\, m_i(t-\tau_t) \tag{15}$$

Substitution of (9) into (15) yields

$$\dot{m}_b(t) = \left\{1 + n\left[\frac{p'(t)}{\bar{p}} - \frac{p'(t-\bar{\tau})}{\bar{p}}\right]\right\}\dot{m}_i(t-\tau_t)$$

or, with a slight modification,

$$\frac{\dot{m}_b(t) - \bar{\dot{m}}+\bar{\dot{m}}}{\bar{\dot{m}}}\bar{\dot{m}} = \left\{1 + n\left[\frac{p'(t)-\bar{p}+\bar{p}}{\bar{p}} - \frac{p'(t-\bar{\tau})-\bar{p}+\bar{p}}{\bar{p}}\right]\right\}\frac{m_i(t-\tau_t)-\bar{\dot{m}}+\bar{\dot{m}}}{\bar{\dot{m}}}\bar{\dot{m}}$$

Denoting

$$\frac{\dot{m}_b(t)-\bar{\dot{m}}}{\bar{\dot{m}}} = \mu_b(t)\ ,\quad \frac{m_i(t-\tau_t)-\bar{\dot{m}}}{\bar{\dot{m}}} = \mu_i(t-\tau_t) \text{ and } \frac{p'(t)-\bar{p}}{\bar{p}} = \phi(t)$$

we have,

$$\mu_b(t) = n\,[\phi(t) - \phi(t-\bar{\tau})] + \mu_i(t-\tau_t) + n[\phi(t) - \phi(t-\bar{\tau})]\mu_i(t-\tau_t)$$

or, approximately,

$$\mu_b(t) \sim \mu_i(t-\tau_t) + n\,[\phi(t) - \phi(t-\bar{\tau})] \tag{16}$$

Introducing the gas residence time

$$\theta_g = Mg/\bar{\dot{m}} \ , \tag{17}$$

as the time an average element of products of combustion will remain inside the chamber in a steady-state operation before it emerges from the nozzle, Eq. (13) becomes

$$\frac{d\phi}{dz} + \mu\ (z) = \mu_b(z) \tag{18}$$

where $z = t/\theta_g$. (19)

The ejection rate can be calculated from the steady-state nozzle transfer function [6] as

$$\mu_e(z) \simeq \phi(z) \tag{20}$$

Substitution of (16) into (18) gives the equation of combustion chamber dynamics.

$$\frac{d\phi}{dz} + \phi(z) = \mu_i(z-\bar{\tau}_t) + n\ [\phi(z) - \phi(z-\bar{\tau})] \tag{21}$$

where τ_t has been approximated by the steady-state value $\bar{\tau}_t$ and has also been non-dimensionalized by the use of θ_g.

The term $\mu_i(z-\bar{\tau}_t)$ in (21) can not be determined without an examination of the mechanics of the feed system of the rocket engine.

Obviously, if the injection rate is independent of the pressure oscillations in the chamber, (21) reduces to its simplest form.

$$\frac{d\phi}{dz} + (1-n)\ \phi(z) = -\ n\ \phi(z-\bar{\tau}) \tag{21}$$

Derivation of Feed System Equation

A schematic feed system for a monopropellant rocket engine as shown as in Fig. 2 can be mathematically represented by several simple component equations, each of which portrays a specific portion of the operation.

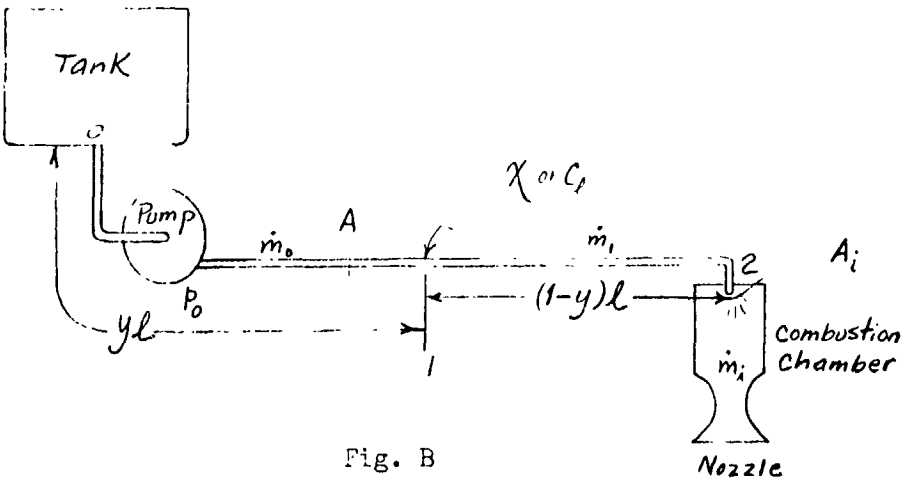

Fig. B

Pump: $$\frac{p_o-\bar{p}_o}{\bar{p}_o} = -D\frac{\dot{m}_o-\bar{\dot{m}}_o}{\bar{\dot{m}}_o} \tag{22}$$

Line 0-1: $$\dot{m}_o-\dot{m}_1 = \rho_o X \frac{dp_1}{dt} \tag{23}$$

$$p_o-p_1 = \frac{yl}{A}\frac{d\dot{m}_o}{dt} \tag{24}$$

Line 1-2: $$p_1-p_2 = \frac{(1-y)l}{A}\frac{d\dot{m}_1}{dt} \tag{25}$$

Injector plate: $$p_2-p_1 = \frac{1}{2}\frac{\dot{m}_i^2}{\rho_o A_i^2} \tag{26}$$

$$\dot{m}_1 = \dot{m}_i \qquad \text{(No feedback control)} \tag{27}$$

where D and X are the proportional constant of the pump and the equivalent spring constant of the feed line, respectively. X is closely related to the feed line capacitance C_ℓ.

H.S. Tsien [3] obtained a differential equation from (22) - (27) which relates the feed system dynamics with the combustion chamber phenomenon.

$$P\left[\phi + DE\left(P + \frac{1}{2}\right)\frac{d\phi}{dz} + JEy\frac{d^2\phi}{dz^2}\right] + \left[1 + D\left(P + \frac{1}{2}\right)\right]\mu_i + \left[DE\left(P + \frac{1}{2}\right) + J\right]\frac{d\mu_i}{dz} + \left[DJE(1-y)\left(P + \frac{1}{2}\right) + JEy\right]\frac{d^2\mu_i}{dz^2} + J^2Ey(1-y)\frac{d^3\mu_i}{dz^3} = 0 \qquad (28)$$

where

$$P = \frac{1}{2}\frac{\bar{p}}{\Delta\bar{p}} \quad \text{(pressure drop parameter)}$$

$$E = \frac{2\Delta\bar{p}\rho_o X}{\dot{\bar{m}}\,\theta_g} \quad \text{(Elasticity parameter)}$$

$$J = \frac{\ell\dot{\bar{m}}}{2\Delta\bar{p}A\theta_g} \quad \text{(Inertia parameter)}$$

Simplification of (28) is possible for specific cases:

I. Constant feed pressure, D = 0

$$P\left(\phi + JEy\frac{d^2\phi}{dz^2}\right) + \mu_i + J\frac{d\mu_i}{dz} + JEy\frac{d^2\mu_i}{dz^2} + J^2Ey(1-y)\frac{d^2\mu_i}{dz^3} = 0 \qquad (29)_I$$

II. Line elasticity or line capacitance concentrated at injector plate, y=1

$$P\left(\phi + JE\frac{d^2\phi}{dz^2}\right) + \mu_i + J\frac{d\mu_i}{dz} + JE\frac{d^2\mu_i}{dz^2} = 0 \qquad (29)_{II}$$

III. Constant feed rate, $D \to \infty$

$$PE \frac{d\phi}{dz} + \mu_i + E \frac{d\mu_i}{dz} + (1-y)\, JE \frac{d^2\mu_i}{dz^2} = 0 \qquad (29)_{III}$$

IV. Line elasticity or Line capacitance concentrated at the tank end of line, $y = 0$.

$$P[\phi + DE(P + \tfrac{1}{2}) \frac{d\phi}{dz}] + [1 + D(P + \tfrac{1}{2})]\mu_i + [DE(P + \tfrac{1}{2}) + J] \frac{d\mu_i}{dz}$$

$$+ DJE\ (P + \tfrac{1}{2}) \frac{d^2\mu_i}{dz^2} = 0 \qquad (29)_{IV}$$

For each special case (four sample cases are shown above) the feed system equation $F(\mu_i, \phi) = 0$ (29) must be solved simultaneously with the chamber equation $C(\phi, \mu_i) = 0$ (21). If one is interested in the stability aspects of the problem, only the characteristic equation is of importance. Some sample analyses leading to this chamber equation will be given below.

Case I. Define a differential operator

$$\mathfrak{D} = 1 + J \frac{d}{dz} + JEy \frac{d^2}{dz^2} + J^2Ey\ (1 - y) \frac{d^3}{dz^3}\ . \qquad (30)$$

Then $(29)_I$ becomes for the instant of $z-\bar{\tau}_t$

$$P\ [1 + JEy \frac{d^2}{dz^2}]\phi_{(z-\bar{\tau})} + \mathfrak{D}\, \mu_{i(z-\bar{\tau}_t)} = 0 \qquad (31)$$

Applying the differential operator $\mathfrak{D}$ defined by (30) into (21) we have

$$\mathfrak{D}\ [(1 - n)\phi(z) - n\phi\ (z-\bar{\tau}) + \frac{d\phi}{dz}] = \mathfrak{D}\ \mu_i(z-\bar{\tau}_t) \qquad (32)$$

Substitution of (32) into (31) yields a differential equation in ϕ only.

$$\left[1 + J\frac{c}{dz^2} + JEy\frac{d^2}{dz^2} + J^2Ey(1-y)\frac{d^3}{dz^3}\right]\left[(1-n)\phi(z) + \frac{d\phi}{dz} - n\phi(z-\bar{\tau})\right]$$

$$+ P\left[1 + JEy\frac{d^2}{dz^2}\right]\phi(z-\bar{\tau}) = 0$$

or

$$\left\{(1-n) + [1 + (1-n)J]\frac{d}{dz} + J[1 + (1-n)Ey]\frac{d^2}{dz^2} + JEy[(1-n)J(1-y) + 1]\frac{d^3}{dz^3}\right.$$

$$\left. + J^2Ey(1-y)\frac{d^4}{dz^4}\right\}\phi(z)$$

$$+ \left[P - n - nJ\frac{d}{dz} + (P-n)JEy\frac{d^2}{dz^2} - nJ^2Ey(1-y)\frac{d^3}{dz^3}\right]\phi(z-\bar{\tau}) = 0 \qquad (33)$$

Equation (33) can be written symbolically

$$L_1[\phi(z)] + L_2[\phi(z-\bar{\tau})] = 0 \qquad (34)$$

where

$$L_1 = (1-n) + [1 + (1-n)J]\frac{d}{dz} + J[1 + (1-n)Ey]\frac{d^2}{dz^2}$$

$$+ JEy[(1-n)J(1-y) + 1]\frac{d^3}{dz^3} + J^2Ey(1-y)\frac{d^4}{dz^4}, \qquad (35)$$

and

$$L_2 = (P-n) - nJ\frac{d}{dz} + (P-n)JEy\frac{d^2}{dz^2} - nJ^2Ey(1-y)\frac{d^3}{dz^3}.$$

Now we relate the function with a retarded variable $(z-\bar{\tau})$ with $\phi(z)$ by the use of Laplace transform, namely,

$$\Phi(s) = \int_0^\infty e^{-sz}\phi(z)\,dz$$

and

$$\int_0^\infty e^{-sz}\,\phi(z-\bar{\tau})\,dz = e^{-s\bar{\tau}}\,\Phi(s) \tag{36}$$

Thus,

$$\Big\{(1-n) + [1 + (1-n)J]s + J\,[1 + (1-n)Ey]s^2 + JEy\,[1 + (1-n)J(1-y)]s^3$$

$$+ J^2Ey(1-y)s^4\Big\}\,\Phi(s) - [1 + (1-n)J]\,\phi(o)$$

$$- [1 + (1-n)Ey]\left[s\phi(o) + \frac{d}{dz}\phi\,\Big|_{z=o}\right]$$

$$-JEy[1 + (1-n)J(1-y)]\left[s^2\phi(o) + s\,\frac{d}{dz}\phi\,\Big|_{z=o} + \frac{d^2}{dz^2}\phi\,\Big|_{z=o}\right]$$

$$-J^2Ey(1-y)\left[s^3\phi(o) + s^2\,\frac{d\phi}{dz}\,\Big|_{z=o} + s\,\frac{d^2}{dz^2}\phi\Big|_{z=o} + \frac{d^3}{dz^3}\phi\Big|_{z=o}\right]$$

$$+ e^{-s\bar{\tau}}\left\{[(P-n) - nJs + (P-n)JEy\,s^2 - nJ^2Ey(1-y)s^3]\,\Phi(s)\right.$$

$$+ nJ\phi(o) - (P-n)JEy\,[s\phi(o) + \frac{d\phi}{dz}\,\Big|_{z=o} +$$

$$\left. + nJ^2Ey(1-y)\,[s^2\phi(o) + s\,\frac{d\phi}{dz}\Big|_{z=o} + \frac{d^2\phi}{dz^2}\,\Big|_{z=o}]\right\} = 0 \tag{37}$$

Solving for $\Phi(s)$, we have

$$\Phi(s) = \phi_1(s)/\phi_2(s) \tag{38}$$

where

$$\phi_1(s) = \left[1 + (1-n)J\right]\phi(0) + \left[1+(1-n)Ey\right]\left[s\phi(0)+\phi'(0)\right] + JEy\left[1+(1-n)J(1-y)\right] \cdot$$

$$\cdot\left[s^2\phi(0)+s\phi'(0)+\phi''(0)\right] + J^2Ey(1-y)\left[s^3\phi(0)+s^2\phi'(0)+s\phi''(0)+\phi'''(0)\right]$$

$$- e^{-s\bar{t}}\left\{nJ\phi(0) - (P-n)JEy\left[s\phi(0)+\phi'(0)\right] + nJ^2Ey(1-y)\left[s^2\phi(0)+s\phi'(0)+\phi''(0)\right]\right\}$$

$$\phi_2(s) = (1-n) + \left[1+(1-n)J\right] s + J\left[1+(1-n)Ey\right]s^2$$
$$+ JEy\left[1+(1-n)J(1-y)\right] s^3 + J^2Ey(1-y)s^4$$
$$- e^{-s\bar{\tau}}\left[(P-n)-nJs+(P-n)JEys^2 - nJ^2Ey(1-y)s^3\right]$$

Eq (38) can now be inverted. The inversion process involves the evaluation of the residues at the poles inside a contour which encloses all the poles of the integrand. Since there are no poles other than those introduced by the vanishing of the denominator, we only need to set it to zero and seek its roots, either real or complex. Hence

$$(1-n)+\left[1+(1-n)J\right] s+J\left[1+(1-n)Ey\right] s^2+JEy\left[1+(1-n)J(1-y)\right] s^3+J^2Ey(1-y)s^4$$
$$= e^{-s\bar{\tau}}\left[(P-n) - nJs + (P-n)\,JEys^2 - nJ^2Ey\,(1-y)s^3\right] \qquad (39)$$

If $y = 1$, such that the line capacitance is concentrated at the injector plate end of the line, (39) further reduces to

$$\frac{(1-n) + \left[1 + (1-n)J\right] s + J\left[1 + (1-n)E\right]s^2 + JES^3}{P - n - nJS + (P-n)\,JEs^2} = e^{-\bar{\tau}s} \qquad (40)$$

For given values of J,E,P,N and $\bar{\tau}$, the roots (either real or complex) can be solved from (40). Since these roots will give rise in the solution $\phi(z)$ to such terms as

$$c_i e^{s_i z} \qquad i = 0,1,2,\ldots\infty \qquad (41)$$

We are certain that a real positive root S_i or a positive real part of a complex root will cause $\phi(z)$ to increase without bound as z increases. In other words, the existence of such a root signifies instability, whereas the existence of a negative real root S_i or a negative real part of a complex root indicates stability.

Case III. Constant feed rate D→∞

$$\text{Define } \mathfrak{D} = 1 + E\frac{d}{dz} + (1-y)\,JE\frac{d^2}{dz^2} \tag{42}$$

then (29)III becomes for the instant of $z - \bar{\tau}_t$

$$PE\frac{d}{dz}\phi(z - \bar{\tau}) + \mathfrak{D}\mu_i(z-\bar{\tau}_t) = 0 \tag{43}$$

But $\mathfrak{D}\mu_i(z - \bar{\tau}_t)$ is, from (21),

$$\mathfrak{D}\mu_i(z - \bar{\tau}_t) = \mathfrak{D}[(1 - n + \frac{d}{dz})\phi(z) + n\phi(z - \bar{\tau})] \tag{44}$$

Hence

$$PE\frac{d}{dz}\phi(z - \bar{\tau}) + [1 + E\frac{d}{dz} + (1 - y)\,JE\frac{d^2}{dz^2}][(1 - n + \frac{d}{dz})\,\phi(z) + n\phi(z - \bar{\tau})] = 0$$

Simplifying,

$$(1 - n + \frac{d}{dz})[1 + E\frac{d}{dz} + (1 - y)\,JE\frac{d^2}{dz^2}]\phi(z)$$

$$+ \{PE\frac{d}{dz} + n[1 + E\frac{d}{dz} + (1 - y)\,JE\frac{d^2}{dz^2}]\}\phi(z - \bar{\tau}) = 0 \tag{45}$$

The counterpart of Eq. (39) for this case is

$$(1 + Es + (1 - y)\,JEs^2)[1 + s - n + n\,e^{-\bar{\tau}s}] + PEs\,e^{-\bar{\tau}s} = 0 \tag{46}$$

Eq. (46) can be solved for s for s real or for s, complex. For real s, we

transpose(46) as

$$e^{-\bar{\tau}s} = -\frac{(1 - n + s)[1 + Es + (1 - y)JEs^2]}{PEs + n[1 + Es + (1 - y)JEs^2]} \tag{47}$$

Graphical procedure must be used to construct curves for the left and right sides of (47) for various values of the parameters n,E,y,J, and P. The intersections of these curves locate the roots. Again, positive roots indicate stability, otherwise, instability.

For s complex, we substitute in (46)

$$s = \alpha + i\omega$$

resulting in

$$e^{-\alpha\bar{\tau}}(\cos \bar{\tau}\omega - i \sin \bar{\tau}\omega) = -\frac{[(1 - n + \alpha)A_1 - \omega A_2] + i[\omega A_1 + (1 - n + \alpha)A_2]}{(PE\alpha + nA_1) + i(PE\omega + nA_2)} \tag{48}$$

where $A_1 = 1 + E\alpha + (1 - y)JE(\alpha^2 - \omega^2)$,

$$A_2 = E\omega + 2(1 - y)JE\alpha\omega. \tag{49}$$

Equate the real and imaginary parts in (48), we obtain

$$-e^{-\alpha\bar{\tau}}\cos \bar{\tau}\omega = \frac{(PE\alpha + nA_1)[(1-n+\alpha)A_1-\omega A_2] + (PE\omega + nA_2)[\omega A_1 + (1-n+\alpha)A_2]}{(PE\alpha + nA_1)^2 + (PE\omega + nA_2)^2}$$

$$e^{-\alpha\bar{\tau}}\sin \bar{\tau}\omega = \frac{(PE\alpha + nA_1)[(1-n+\alpha)A_2 + \omega A_1] - (PE\omega + nA_2)[-\omega A_2 + (1-n+\alpha)A_1]}{(PE\alpha + nA_1)^2 + (PE\omega + nA_2)^2} \tag{50}$$

Further simplification yields

$$-\tan \bar{\tau}\omega = \frac{(PE\alpha + nA_1)\,\omega A_1 + (1-n+\alpha)A_2 - (PE\omega + nA_2)\,(1-n+\alpha)A_1 - \omega A_2}{-(PE\alpha + nA_1)\,\omega A_2 - (1-n+\alpha)A_1 + (PE\omega + nA_2)\,(1-n+\alpha)A_2 - \omega A_1} \tag{51}$$

$$e^{-2\alpha\bar{\tau}} = \frac{[(1 - n + \alpha)^2 + \omega^2][A_1^2 + A_2^2]}{(PE\alpha + nA_1)^2 + (PE\omega + nA_2)^2} \tag{52}$$

The case of neutral stability is characterized by $\alpha = 0$. Setting $\alpha = 0$ in (51) and (52) we obtain

$$-\tan \bar{\tau}\omega = \frac{nA_1^\circ[\omega A_1^\circ + (1 - n)A_2^\circ] - (PE\omega + nA_2^\circ)[(1 - n)A_1^\circ - \omega A_2^\circ]}{-nA_1^\circ[\omega A_2^\circ - (1 - n)A_1^\circ] + (PE\omega + nA_2^\circ)[(1 - n)A_2^\circ - \omega A_1^\circ]} \tag{53}$$

$$1 = \frac{[(1 - n)^2 + \omega^2][(A_1^\circ)^2 + (A_2^\circ)^2]}{(nA_1^\circ)^2 + (PE\omega + nA_2^\circ)^2} \tag{54}$$

where $A_1^\circ = 1 - J'E\omega^2$

$A_2^\circ = E\omega$

$J' = (1 - y)J$.

Simplifying, (53), (54) becomes

$$-\tan \bar{\tau}\omega = \frac{\omega\psi - (1 - n) + (P + n)\left[\frac{\omega}{n\psi} + \frac{1 - n}{n}\right]}{\omega + (1 - n)\psi + (P + n)\left[\frac{\omega}{n} + \frac{1 - n}{n\psi}\right]} \tag{55}$$

and

$$(P + n)^2 - n^2 = [\omega^2 + (1 - n)^2 - n^2](\psi^2 + 1) \tag{56}$$

where

$$\psi = J\omega - \frac{1}{E\omega}.$$

THE PRESENT MODEL

The low frequency combustion stability model described here is an extension of Crocco and Cheng's (4) analysis of the monopropellant system to the bipropellant case. The model considers the injector capacitance and inertance as well as the resistance of both propellant systems and allows for separate and distinct time lags for each propellant. Previous bipropellant models do not consider the effects of injector capacitance and inertance. The time lags are the time intervals between the fuel and oxidizer injection and the assumed sudden conversion to exhaust products; they include all the physical and chemical processes in the conversion such as heating, vaporization, mixing, and reaction.

ANALYSIS

The monopropellant, single time lag model of Crocco and Cheng is modified to accommodate the bipropellant case by adding a term accounting for the second propellant to the equation governing the dynamics of the gas flow in the combustion chamber and adding a new equation representing the dynamics of the second feed system. The modified equation for the chamber dynamics in dimensionless form is

$$\frac{d}{dt}\,\delta p_c(t) + \delta p_c(t) = \delta \dot{W}_o\,(t - \tau_o) + \delta \dot{W}_f\,(t - \tau_f) + n\,[\,\delta p_c(t) - \delta p_c(t-\tau)] \tag{57}$$

assuming the the pressure and temperature at any given instant are constant throughout the combustion chamber and the time lag is constant for all propellant elements. The dimensionless chamber pressure, P_c and flow rates $\dot{w}_o$ and $\dot{w}_f$ are

defined in terms of their steady-state values and the dimensionless time, t, time lags for the oxidizer and the fuel, τ_o and τ_f, and sensitive time lag, $\bar{\tau}$, are defined in terms of the gas residence time, θ_g. (Symbols are listed at the front of the report and θ_g is defined in Appendix A.)

Two dimensionless equations representing the dynamics of the feed system, one for the oxidizer and one for the fuel assuming constant feed pressure at the injector inlet and all capacitance and inertance located at the injector are

$$P_o(1+J_oE_oD^2)\,\delta p_c(t) + (1+J_oD + J_oE_oD^2)\,\delta\dot{W}_o(t) = 0 \tag{58}$$

$$P_f(1+J_fE_fD^2)\,\delta p_c(t) + (1+J_fD + J_fE_fD^2)\,\delta\dot{W}_f(t) = 0 \tag{59}$$

where D is a differential operator, and the dimensionless inertance, J_o and J_f, capacitance E_o and E_f and pressure drop parameters, P_o and P_f, are defined in Appendix A. Substituting equations 2 and 3 into equation 1 and applying Laplace transformation to the result yields

$$\begin{aligned}&[S+1-n+ne^{-\tau s}][1+J_oS+J_oE_oS^2][1+J_fS+J_fE_fS^2]\\ &= -e^{-\tau_o S}P_o[1+J_oE_oS^2]\,[1+J_fS+J_fE_fS^2] - e^{-\tau_f S}P_f[1+J_fE_fS^2]\,[1+J_oS+J_oE_oS^2]\end{aligned} \tag{60}$$

Substituting $\alpha+i\omega$ for S in equation (60) and equating the real and imaginary parts of both sides results in two simultaneous equations,

$$\begin{aligned}(GH-KN)(\alpha+1)-(KH+GN)\omega = &-P_o e^{-\alpha\tau_o}\left\{\cos\omega\tau_o[MH-N(2\alpha\omega J_oE_o)] + \sin\omega\tau_o[MH+H(2\alpha\omega J_oE_o)]\right\}\\ &-P_f e^{-\alpha\tau_f}\left\{\cos\omega\tau_f[RG-K(2\alpha\omega J_fE_f)] + \sin\omega\tau_f[KR+G(2\alpha\omega J_fE_f)]\right\}\end{aligned} \tag{61}$$

$$\begin{aligned}(GH-KN)\omega + (KH+GN)\,(\alpha+1) = &-P_o e^{-\alpha\tau_o}\left\{\cos\omega\tau_o[MN+H(2\alpha\omega J_oE_o)]\right.\\ &\left.-\sin\omega\tau_o[MH-N(2\alpha\omega J_oE_o)]\right\}\\ &-P_f e^{-\alpha\tau_f}\left\{\cos\omega\tau_f[KR+G(2\alpha\omega J_fE_f)] - \sin\omega\tau_f[RG-K(2\alpha\omega J_fE_f)]\right\}\end{aligned} \tag{62}$$

where: $G = 1 + J_o\alpha + J_oE_o(\alpha^2 - \omega^2)$

$H = 1 + J_f\alpha + J_fE_f(\alpha^2 - \omega^2)$

$K = J_o\omega + 2J_oE_o\alpha\omega$

$N = J_f\omega + 2J_fE_f\alpha\omega$

$M = 1+J_oE_o(\alpha^2-\omega^2)$

$R = 1+J_fE_f(\alpha^2-\omega^2)$

For reasons to be stated later, the interaction index n and the vaporization time $\bar{\tau}$ have been set to zero in Equations (61) and (62).

Equations (61) and (62) can be solved simultaneously† for α and ω to evaluate the stability of any combustor design once the pressure drop, inertance, capacitance and time lags are known*. The magnitude of α indicates incidentally, the proneness of the system to instability (if $\alpha>o$) or to stability (if $\alpha<o$).

The time lags, τ_o and τ_f are by Crocco's definition the total time lags and are composed of a constant, steady-state (insensitive) portion and a variable (sensitive) portion $\bar{\tau}$. Rigorous analyses would take into account this time-dependent or sensitive portion of the time lag; however, for most applications it can be neglected because it is small compared to the total time lag. Once the sensitive time lag is taken as zero it follows that the interaction index must also be zero because zero sensitive time lag requires that the burning rate be independent of chamber pressure.

---

† The programs written for this purpose are listed in Appendix C. The calculations which underlie the solutions for α and ω are discussed in Appendix B.

* The curves showing variations of α with L_o (V_o) while L_F (V_F) is held constant are shown in Figures C (D).

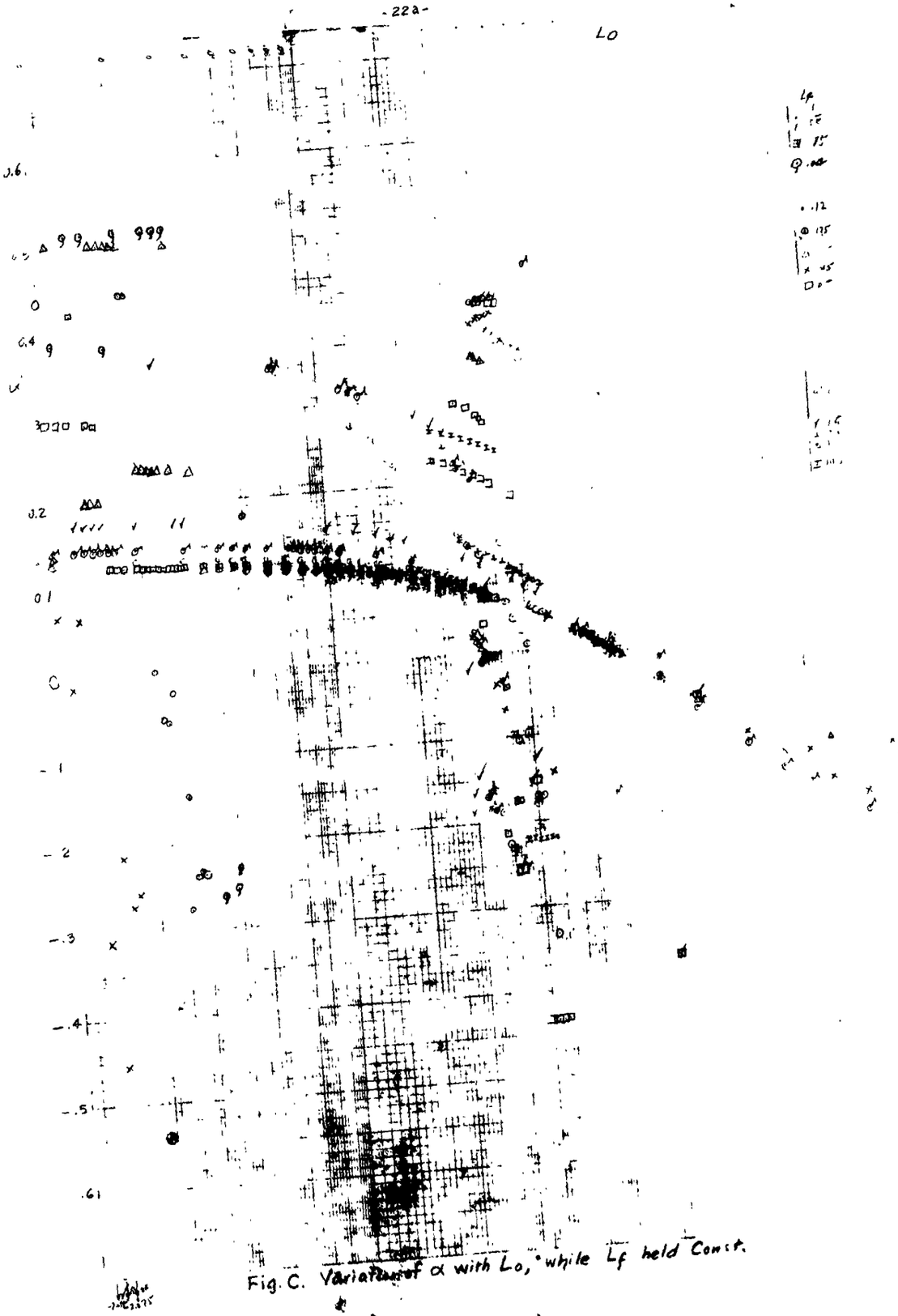

Fig. C. Variation of α with L_o, while L_f held Const.

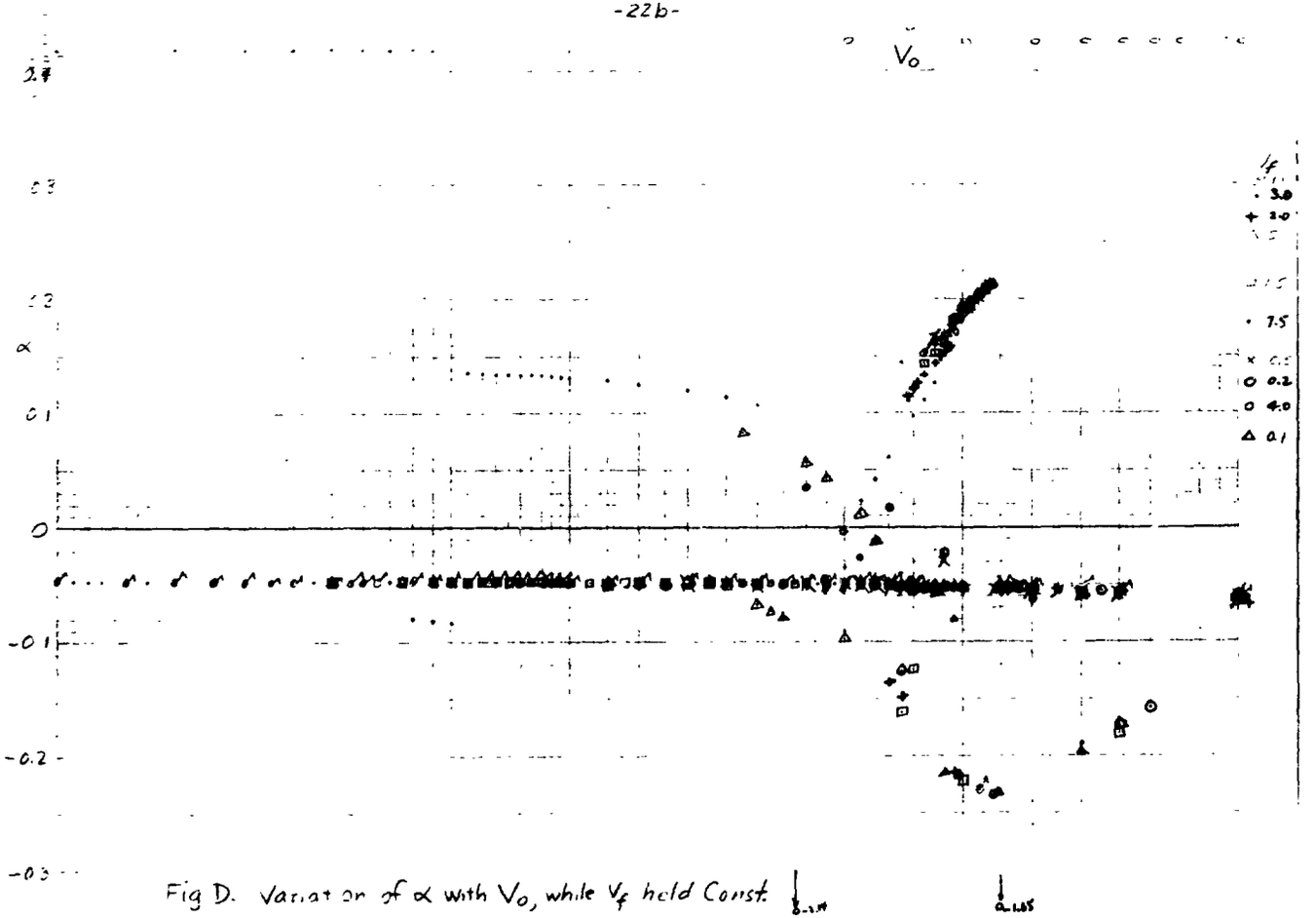

Fig D. Variation of α with V_o, while V_f held Const.

The total time lag is defined as the time increment between injection of a propellant and its conversion into combustion products. Certainly this time lag is not the same for all propellant elements. It is therefore customary to define an average time lag for each propellant which may be done by determining the lapsed travel time between injection and the axial position where combustion is assumed to take place. The methods of Priem [7] can be used to determine the position of the combustion front.

DISCUSSIONS AND RESULTS

In order to illustrate the effects of capacitance, inertance and resistance of the systems on stability, equations 5 and 6 were solved for the neutral stability boundaries ($\alpha = 0$). Figures 1 through 3 show the neutral stability boundaries in terms of the fuel and oxidizer orifice lengths for three different oridizer pressure drops. Fuel and oxidizer cavity volume, fuel pressure drop and time lags are held constant. Figures 4 and 5 show the neutral stability boundaries for two different fuel pressure drops while oxidizer pressure drop is held constant along with the cavity volumes and time lags. Because more than one pair of roots satisfy equations 5 and 6 multiple stable and unstable zones exist. The fuel and oxidizer pressure drops affect these zones but unfortunately no trends are apparent.

Figures 6 through 8 show the neutral stability boundaries in terms of the fuel and oxidizer cavity volumes for three different exidizer pressure drops. Fuel and oxidizer orifice lengths, fuel pressure drop and time lags are held constant. Figures 9 and 10 show the neutral stability boundaries for two different fuel pressure drops while oxidizer pressure drop is held constant along with the orifice lengths and time lags. Although multiple stable and unstable zones exist as in figures 1 through 5, it appears that intermediate values of oxidizer and fuel pressure drops (figures 7 and 9, respectively) result in the narrowest unstable zones. Thus, if an operating point were selected which is in an unstable zone of figure 6, the system could be stabilized by reducing either the oxidizer pressure drop to 124 psi, or the fuel pressure drop to 87 psi (figures 7 and 9). Further reduction in either oxidizer or fuel pressure drop results in the return to unstable operation. This result cannot be predicted by either single time lag models or double time lag models which do not include injector inertance and capacitance.

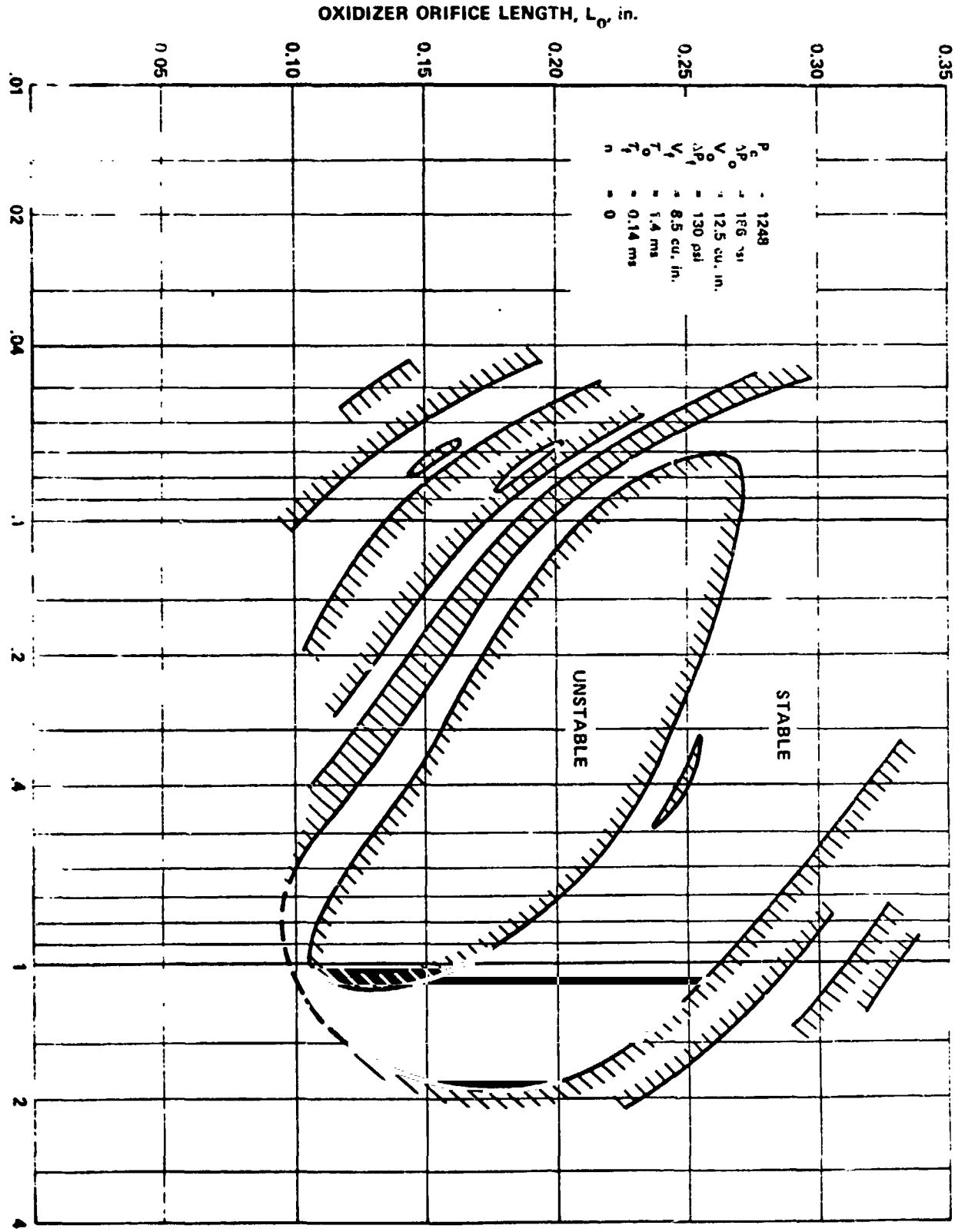

Fig. 1. FUEL ORIFICE LENGTH, L_f, in.

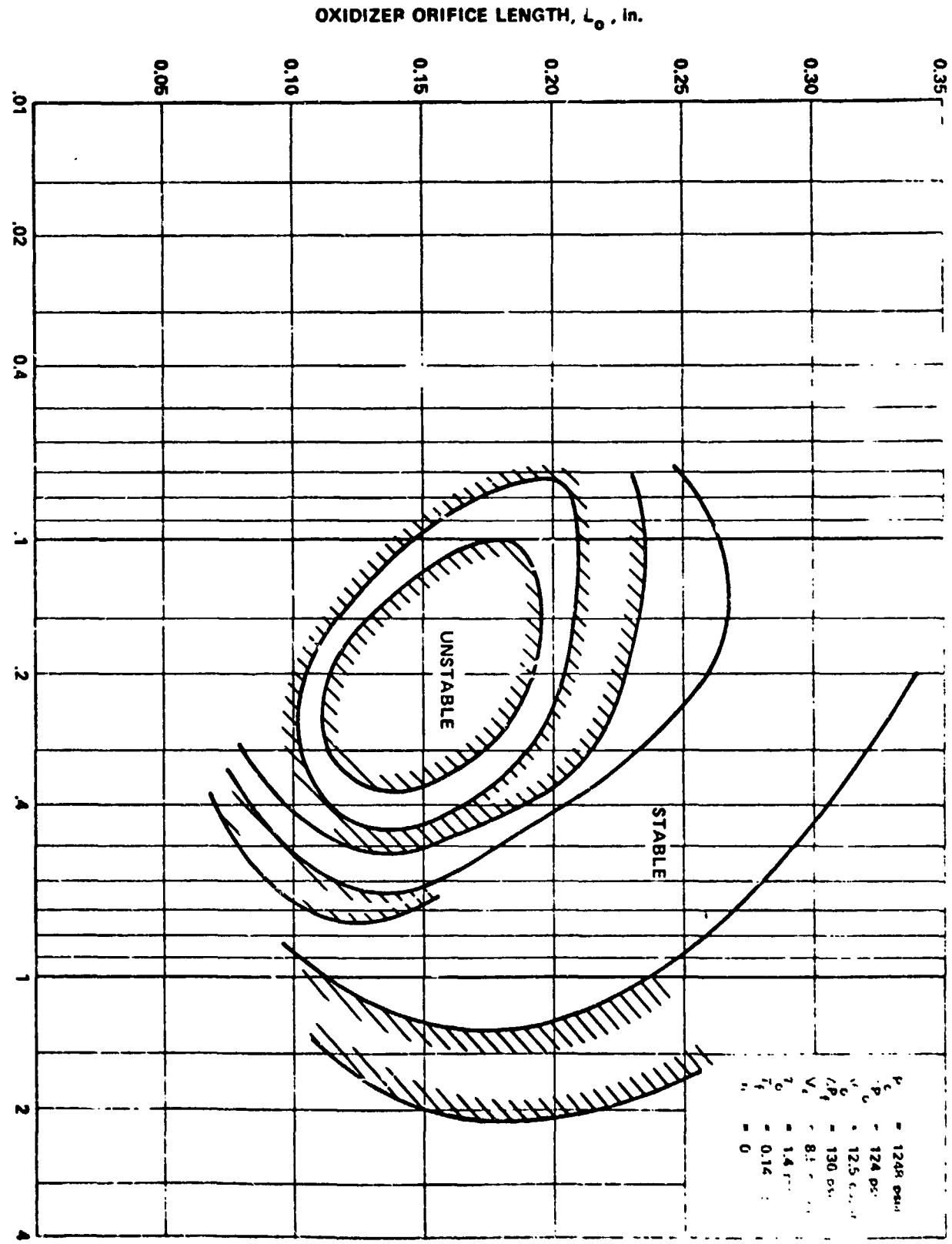

Fig. 2. FUEL ORIFICE LENGTH, L_f, in.

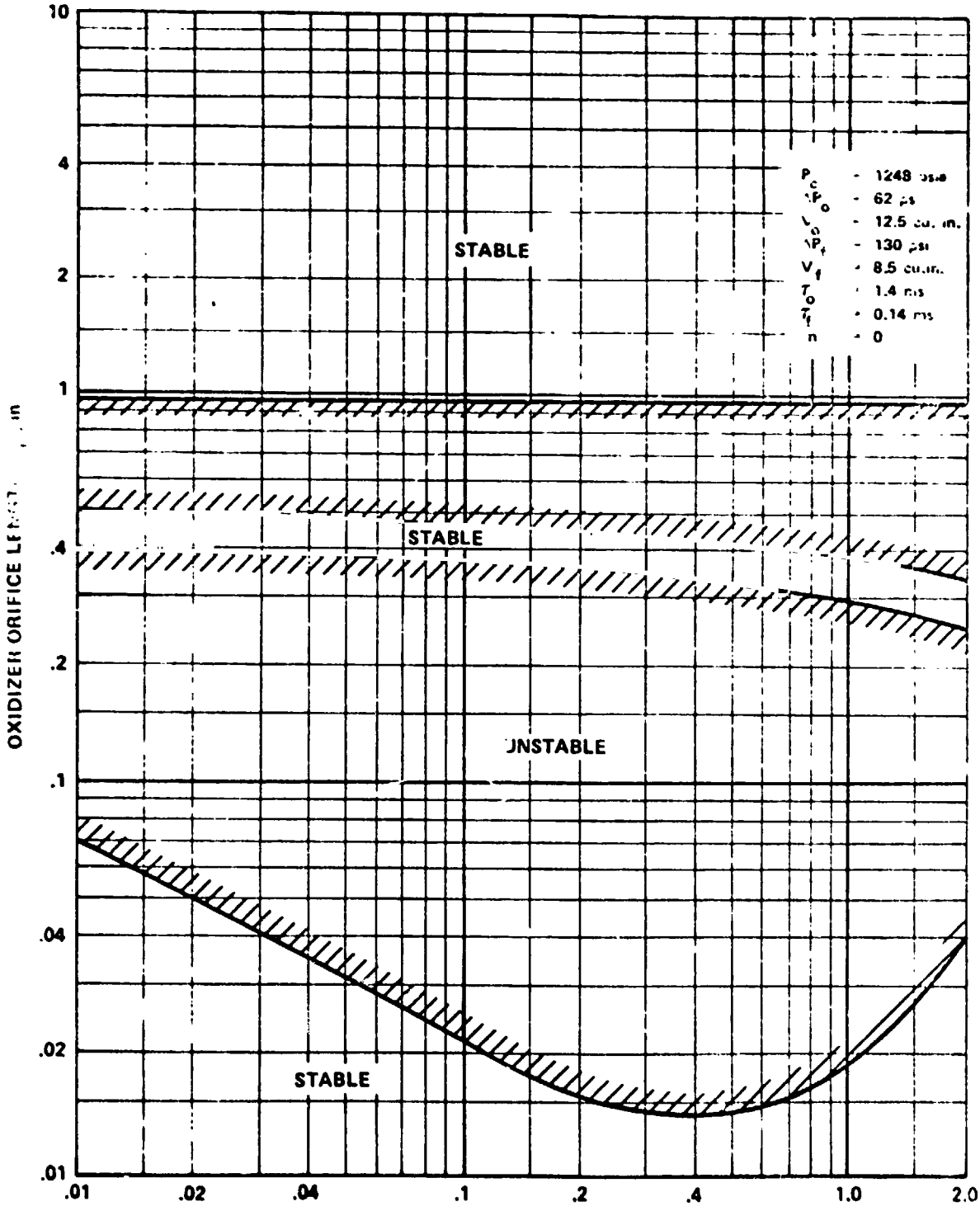
10
4
2
1
.4
.2
.1
.04
.02
.01
.01
.02
.04
.1
.2
.4
1.0
2.0
STABLE
STABLE
UNSTABLE
STABLE
P_c - 1248 psia
ΔP_o - 62 psi
V_o - 12.5 cu. in.
ΔP_f - 130 psi
V_f - 8.5 cu.in.
τ_o - 1.4 ms
τ_f - 0.14 ms
n - 0
OXIDIZER ORIFICE LE
FUEL ORIFICE LENGTH, L_f, in.

Fig. 3.

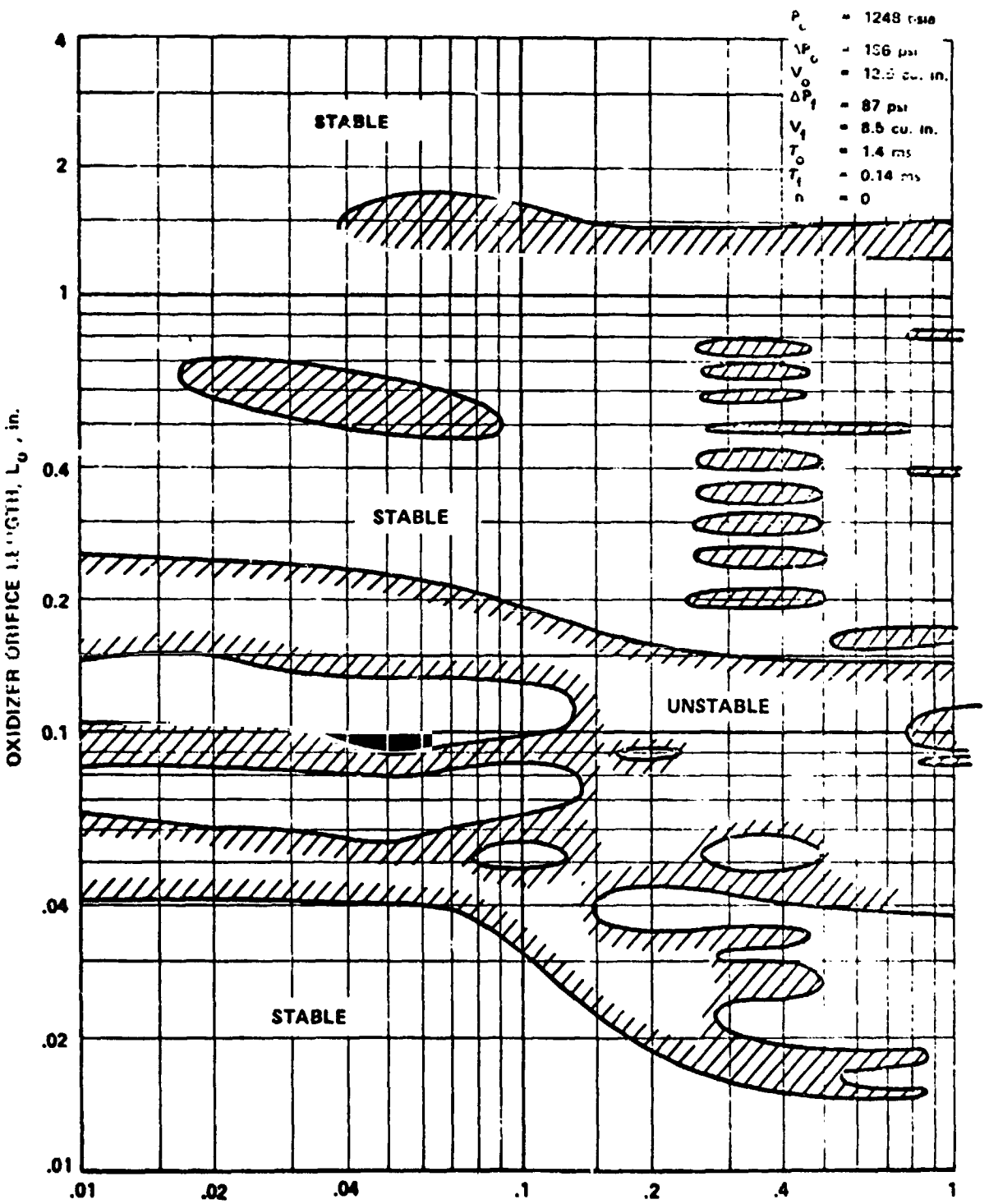

Fig. 4. FUEL ORIFICE LENGTH, L_f, in.

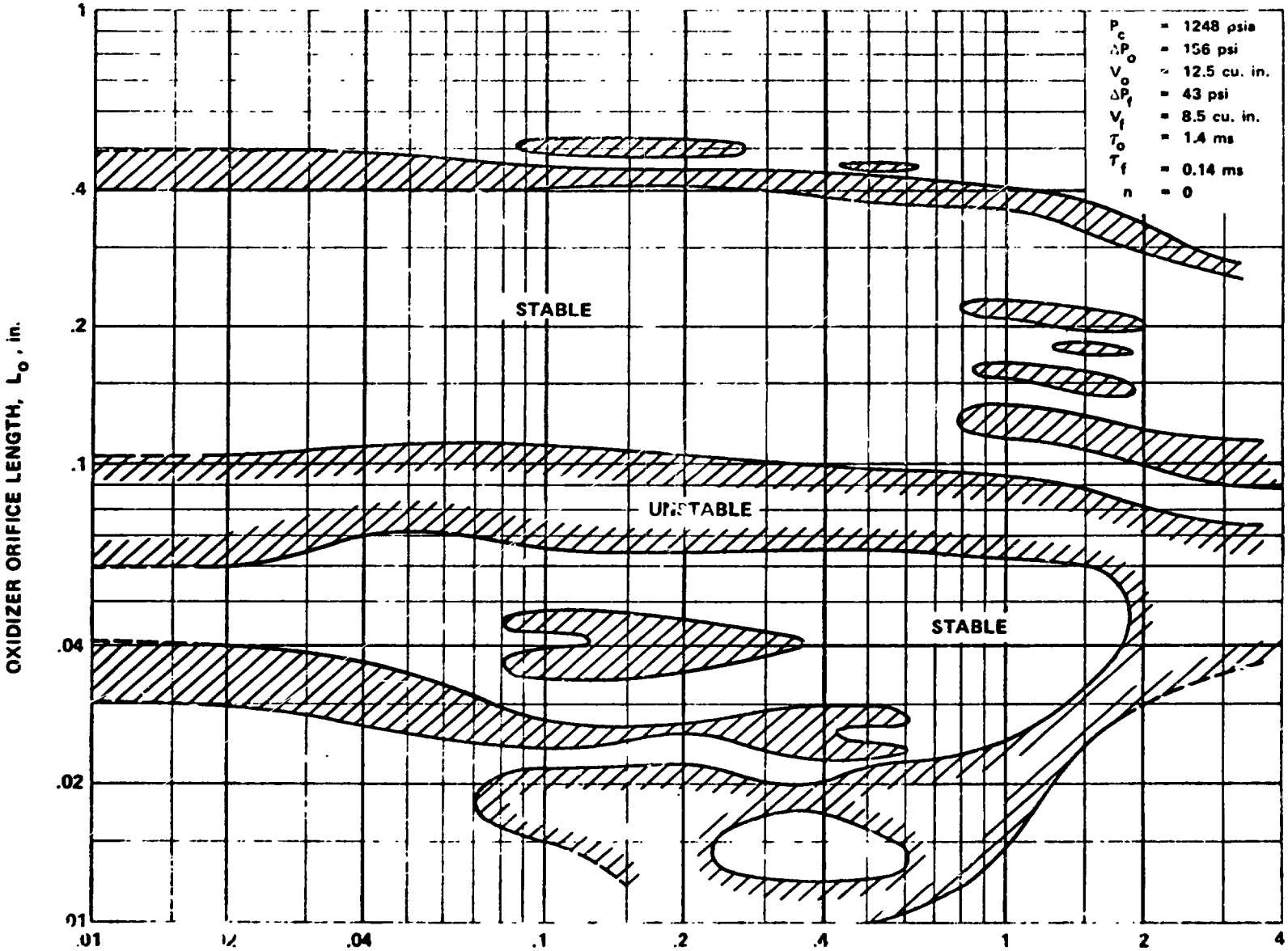

Fig. 5. FUEL ORIFICE LENGTH, L_f, in.

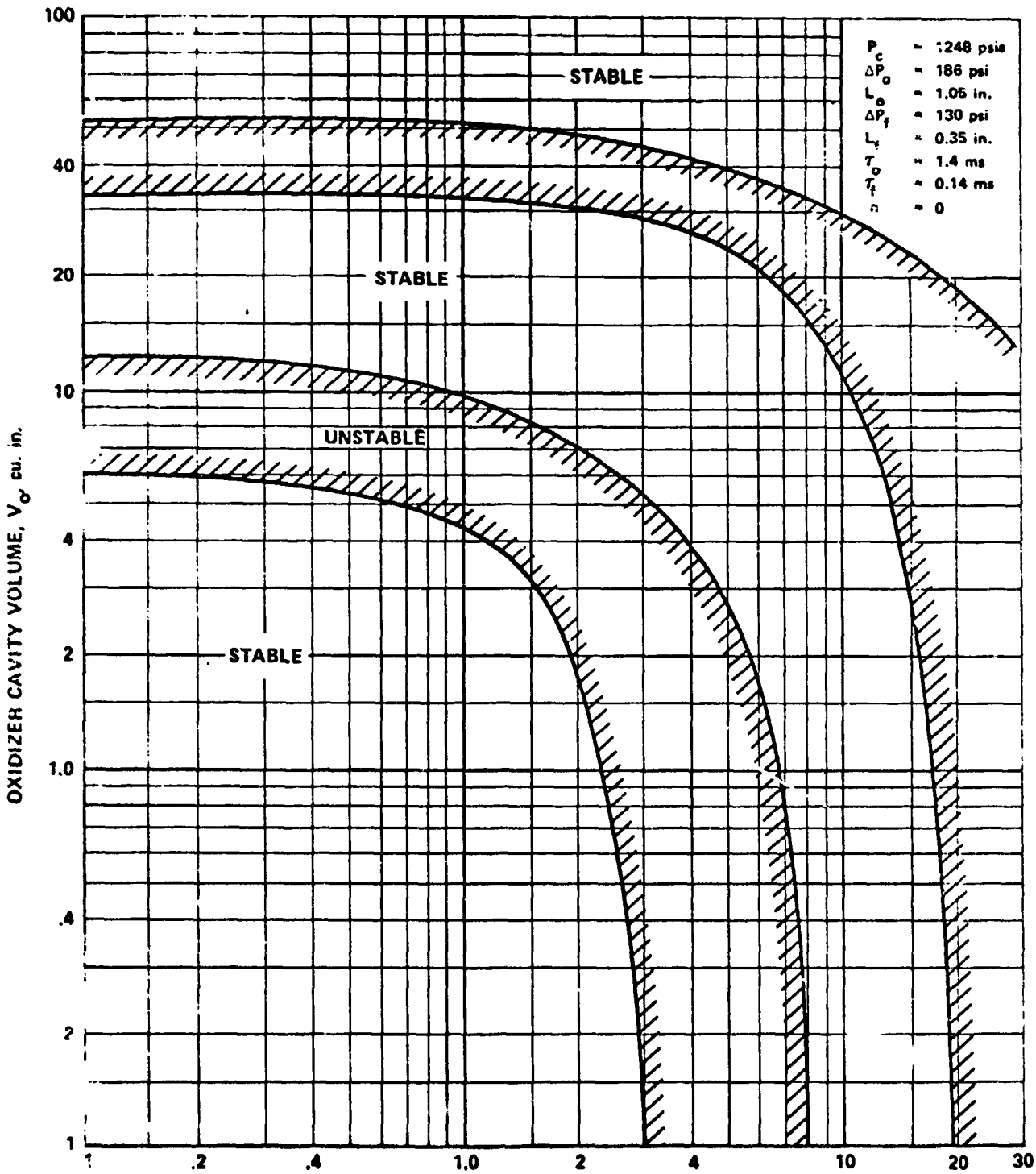

Fig. 6. **FUEL CAVITY VOLUME, V_f, cu. in.**

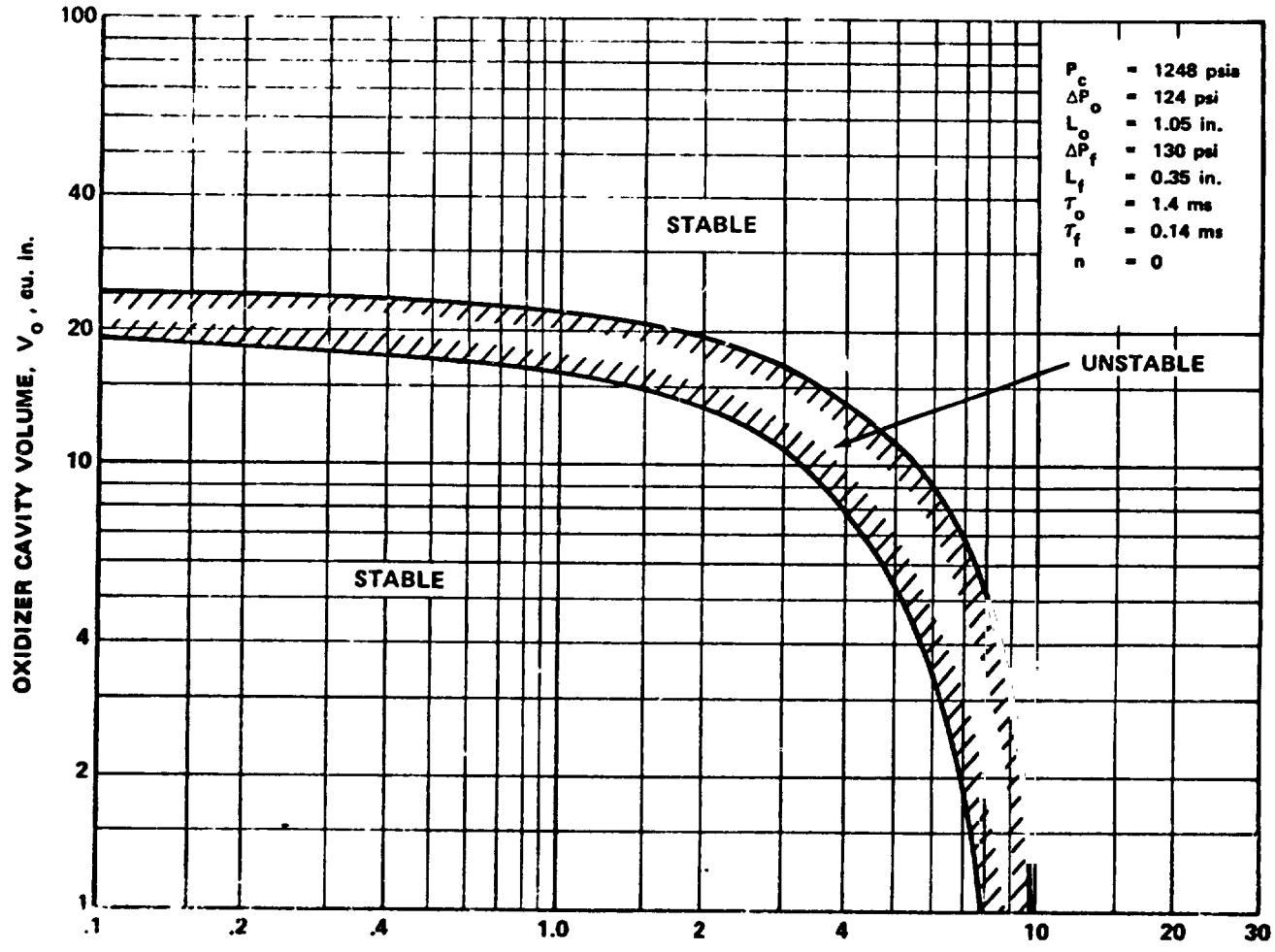

Fig. 7. FUEL CAVITY VOLUME, V_f, cu. in.

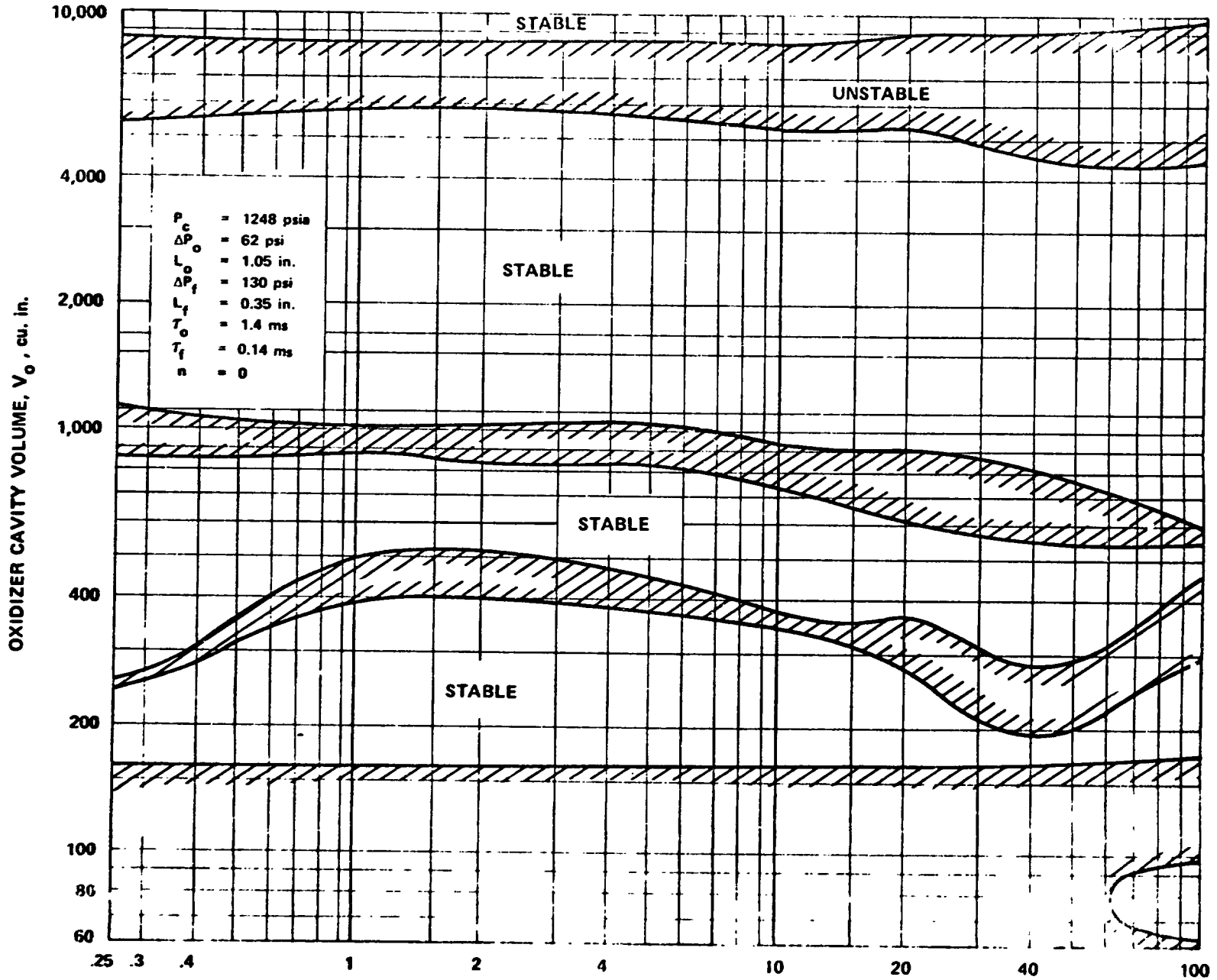
STABLE
UNSTABLE
STABLE
STABLE
STABLE
P_c = 1248 psia
ΔP_o = 62 psi
L_o = 1.05 in.
ΔP_f = 130 psi
L_f = 0.35 in.
τ_o = 1.4 ms
τ_f = 0.14 ms
n = 0
OXIDIZER CAVITY VOLUME, V_o, cu. in.
10,000
4,000
2,000
1,000
400
200
100
80
60
.25
.3
.4
1
2
4
10
20
40
100
FUEL CAVITY VOLUME, V_f, cu. in.

Fig. 8.

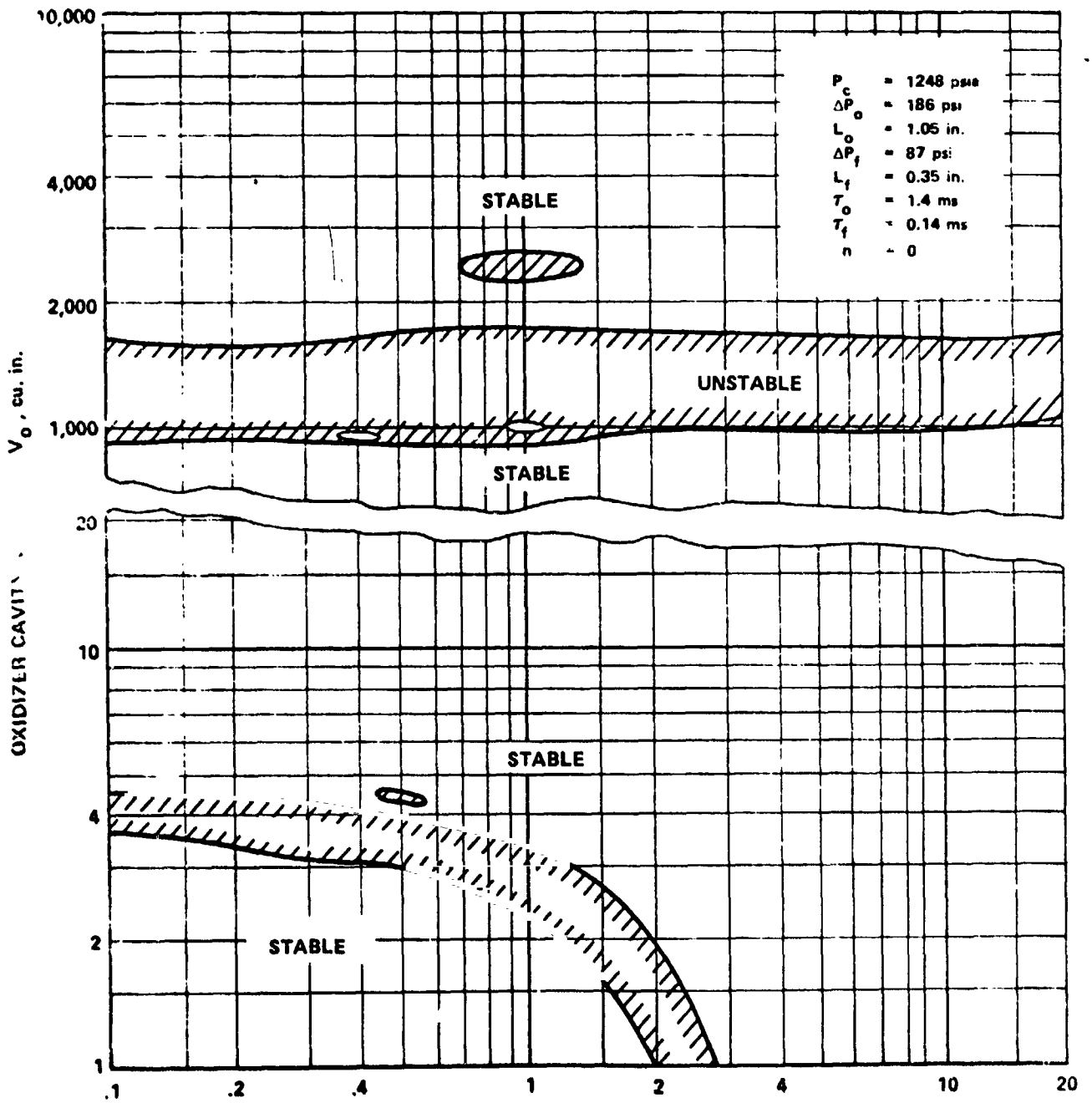

Fig. 9. FUEL CAVITY VOLUME, V_f, cu. in.

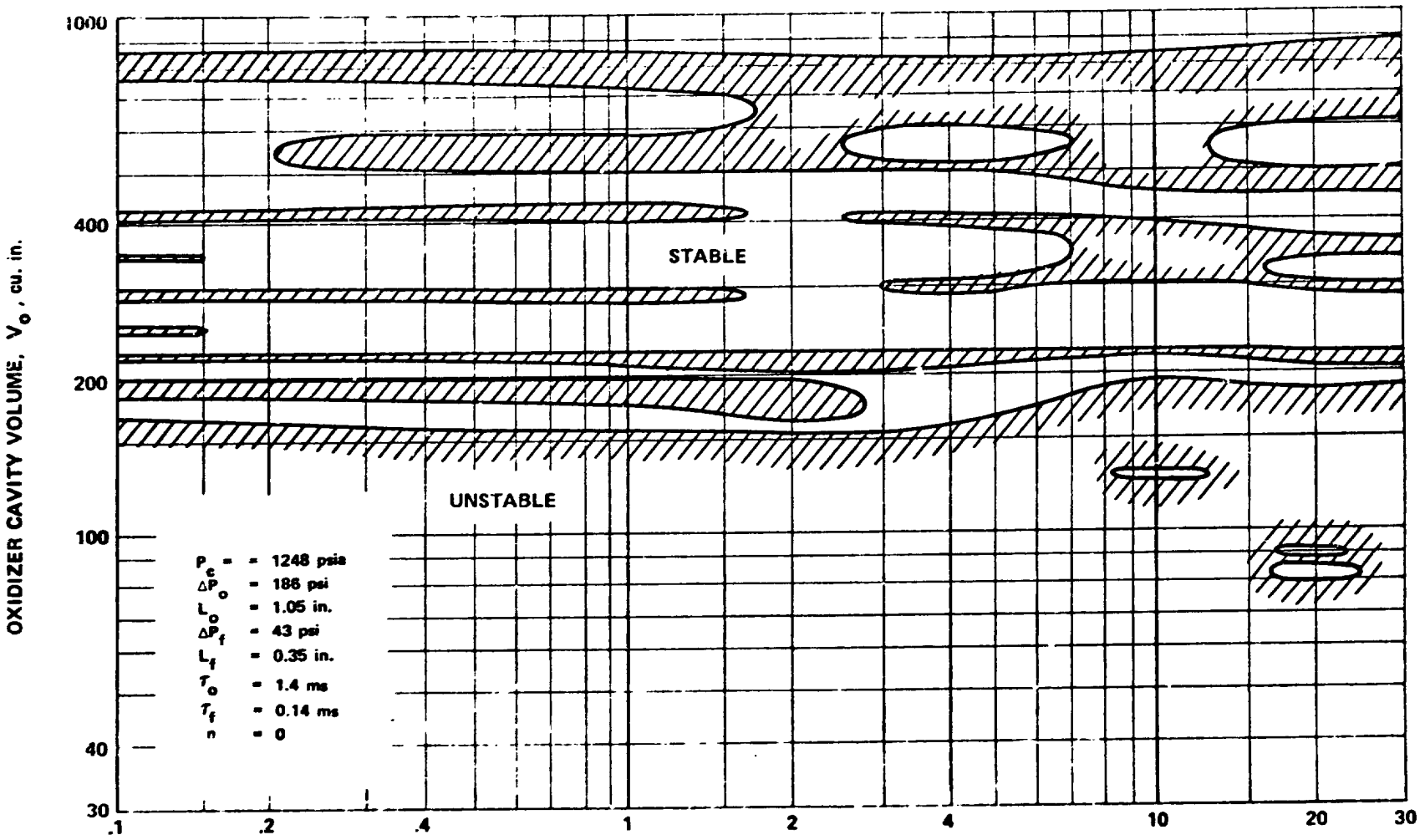

Fig. 10. FUEL CAVITY VOLUME, V_f, cu. in.

CONCLUSIONS

The contribution advanced by the stability model described here is the inclusion of injector inertance and capacitance in addition to resistance in the analysis of bipropellant rocket systems with different time lags. Neutral stability boundaries are shown in terms of these parameters in order to demonstrate their interactions.

This model provides a method of designing a stable system by optimizing the pertinent design variables rather than maximizing the pressure drop and ignoring the others which has been the traditional approach. This model suggests that in some cases stability can be enhanced by reducing pressure drop, and therefore maintaining pressure drop to chamber pressure ratio is not necessarily desirable.

REFERENCES

1. Summerfield, Martain, "A Theory of Unstable Combustion in Liquid Propellant Rocket Systems." J. Am. Rocket Soc., Vol. 21, No. 5, Sept. 1951, pp. 108-114.

2. Gunder, D.F., and Friant, D.R., "Stability of Flow In a Rocket Motor." J. Appl. Mech., Vol. 17, No. 3, Sept. 1950, pp. 327-333.

3. Crocco, Luigi and Cheng, Sin-I. Theory of Combustion Instability in Liquid Propellant Rocket Motors. London: AGARDograph No. 8, Butterworths Sci. Pub., 1956.

4. Hurrell, Herbert G., "Analysis of Injection-Velocity Effects on Rocket Motor Dynamics and Stability." NASA TR R-43, 1959.

5. Wenzel, L.M. and Szuch, J.R., "Analysis of Chugging in Liquid-Bipropellant Rocket Engines Using Propellants with Different Vaporization Rates." NASA TN D-3080, 1965.

6. Tsien, H.S., "The Transfer Functions of Rocket Nozzles". Jl. Amer. Rocket Society 22 (1952) 139, 172. Also pp. 31 of 3 .

7. Priem, R.J. and Heidmann, M.F., "Propellant Vaporization as a Design Criterion for Rocket Engine Combustion Chambers." NASA TR R-67, 1960.

Subscript

c	Combustion chamber
o	Oxidizer
f	Fuel
i	Initial

Superscript

*	Indicates dimensional quantities

LIST OF SYMBOLS

SYMBOL	DEFINITION
D	Differential operator, d/dt
E	Dimensionless elasticity parameter
J	Dimensionless inertia parameter
P	Dimensionless pressure drop parameter
p^*	Pressure
p	Dimensionless pressure
M	Molecular weight
V	Volume
T	Temperature
$\dot{m}$	Mass flow rate
R	Universal gas constant
p	Pressure drop
ρ	Density
X	Compliance
θ_g	Gas residence time
l	Injector orifice length
A	Injector orifice area
s	Laplace transform variable
$\dot{w}$	Weight flow rate
t	Dimensionless time
n	Interaction index
α	Dimensionless Damping Coefficient
α^*	Damping Coefficient
ω	Dimensionless frequence
ω^*	Frequency
τ	Dimensionless time lag
τ^*	Time lag
$\bar{\tau}$	Dimensionless sensitive time lag
$\bar{\tau}^*$	Sensitive time lag
i	$\sqrt{-1}$

Appendix A

Definition of Parameters

The gas residence time, θ_g is used to nondimensionalize many of the quantities used in the analysis. It is defined as

$$\theta_g = \frac{V_c \rho_c}{\dot{m}} = \frac{V_c \rho_c M_c}{R T_c \dot{m}}$$

The pressure drop parameter, P is defined as

$$P = \frac{\rho_c}{2\Delta\rho}$$

The elasticity parameter, E is defined as

$$E = \frac{2\Delta p \rho X}{\dot{m}\ \theta_g}$$

The inertia parameter, J is defined as

$$J = \frac{\ell\ \dot{m}}{2\Delta p A \theta_g}$$

The real and imaginary parts of the Laplace transform variable S (α and ω), the oxidizer and fuel combustion delays, and the sensitive time lag are nondimensionalized by the use of the gas residence time, θ_g, namely,

$$\alpha = \alpha^* \theta_g$$

$$\omega = \omega^* \theta_g$$

$$\tau_o = \tau_o^* / \theta_g$$

$$\tau_f = \tau_f^* / \theta_g$$

$$\bar{\tau} = \bar{\tau}^* / \theta_g$$

Appendix B

Solution of Equations (61) and (62) by Newton-Raphson Method

For convenience, Equations (61) and (62) are denoted, symbolically and respectively, as

$$f(\alpha,\omega) = 0 \tag{A-1}$$

$$g(\alpha,\omega) = 0 \tag{A-2}$$

By series expansion, Equations (1) and (2) are rewritten

$$f(\alpha,\omega) = f(\alpha_{n-1},\omega_{n-1}) + (\alpha-\alpha_{n-1}) \frac{\partial f}{\partial \alpha} (\alpha_{n-1},\omega_{n-1}) + (\omega-\omega_{n-1}) \frac{\partial f}{\partial \omega} (\alpha_{n-1},\omega_{n-1}) \tag{A-3}$$

$$g(\alpha,\omega) = g(\alpha_{n-1},\omega_{n-1}) + (\alpha-\alpha_{n-1}) \frac{\partial g}{\partial \omega} (\alpha_{n-1},\omega_{n-1}) + (\omega-\omega_{n-1}) \frac{\partial g}{\partial \omega} (\alpha_{n-1},\omega_{n-1}) \tag{A-4}$$

where α_{n-1}, ω_{n-1} are the values of α and ω at stage of computation n-1.
Now if at a subsequent stage n, where $\alpha = \alpha_n$ and $\omega = \omega_n$ the right-hand sides of (3) and (4) vanish, the following can be written immediately.

$$\alpha_n \frac{\partial f}{\partial \alpha} (\alpha_{n-1},\omega_{n-1}) + \omega_n \frac{\partial f}{\partial \omega} (\alpha_{n-1},\omega_{n-1}) = -f(\alpha_{n-1},\omega_{n-1}) + \alpha_{n-1} \frac{\partial f}{\partial \alpha} (\alpha_{n-1},\omega_{n-1}) + \omega_{n-1} \frac{\partial f}{\partial \omega} (\alpha_{n-1},\omega_{n-1}) \tag{A-5}$$

$$\alpha_n \frac{\partial g}{\partial \alpha} (\alpha_{n-1},\omega_{n-1}) + \omega_n \frac{\partial g}{\partial \omega} (\alpha_{n-1},\omega_{n-1}) = -g(\alpha_{n-1},\omega_{n-1}) + \alpha_{n-1} \frac{\partial g}{\partial \alpha} (\alpha_{n-1},\omega_{n-1}) + \omega_{n-1} \frac{\partial g}{\partial \omega} (\alpha_{n-1},\omega_{n-1}) \tag{A-6}$$

Written in matrix form, (5) and (6) take the form

$$\begin{bmatrix} \frac{\partial f}{\partial \alpha} & \frac{\partial f}{\partial \omega} \\ \frac{\partial g}{\partial \alpha} & \frac{\partial g}{\partial \omega} \end{bmatrix}_{n-1} \begin{bmatrix} \alpha_n \\ \omega_n \end{bmatrix} = - \begin{bmatrix} f \\ g \end{bmatrix}_{n-1} + \begin{bmatrix} \frac{\partial f}{\partial \alpha} & \frac{\partial f}{\partial \omega} \\ \frac{\partial g}{\partial \alpha} & \frac{\partial g}{\partial \omega} \end{bmatrix}_{n-1} \begin{bmatrix} \alpha_{n-1} \\ \omega_{n-1} \end{bmatrix} \tag{A-7}$$

Inversion of (7) yields

$$\begin{bmatrix} \alpha_n \\ \omega_n \end{bmatrix} = - \begin{bmatrix} \frac{\partial f}{\partial \alpha} & \frac{\partial f}{\partial \omega} \\ \frac{\partial g}{\partial \alpha} & \frac{\partial g}{\partial \omega} \end{bmatrix}^{-1}_{n-1} \begin{bmatrix} f \\ g \end{bmatrix}_{n-1} + \begin{bmatrix} \alpha_{n-1} \\ \omega_{n-1} \end{bmatrix}$$

$$= \begin{bmatrix} \alpha_{n-1} \\ \omega_{n-1} \end{bmatrix} - \frac{1}{DFG} \begin{bmatrix} \frac{\partial g}{\partial \omega} & -\frac{\partial f}{\partial \omega} \\ -\frac{\partial g}{\partial \alpha} & \frac{\partial f}{\partial \alpha} \end{bmatrix}_{n-1} \begin{bmatrix} f \\ g \end{bmatrix}_{n-1} \tag{A-8}$$

where

$$DFG = \begin{bmatrix} \frac{\partial f}{\partial \alpha} & \frac{\partial f}{\partial \omega} \\ \frac{\partial g}{\partial \alpha} & \frac{\partial g}{\partial \omega} \end{bmatrix}_{n-1} \tag{A-9}$$

Iteration follows until the roots α and ω are pin-pointed within desired accuracy.

Such a scheme of solving simultaneous equations is known as the Newton-

Raphson method.

A computer program was developed such that for given parameters for a specific rocket engine, for instance,

$P_0 = 3.36$, $P_f = 4.82$, $J_0 = 1.189$, $E_0 = 0.2018$,

$\tau_0 = 5.2692$, $\tau_f = 0.4$, $J_f = 0.061$, $E_f = 0.233$,

the fundamental roots are obtained

$$\alpha = -0.112$$

$$\omega = 0.49.$$

Other examples are solved similarly and the results of computation are shown in Figs. i and ii.

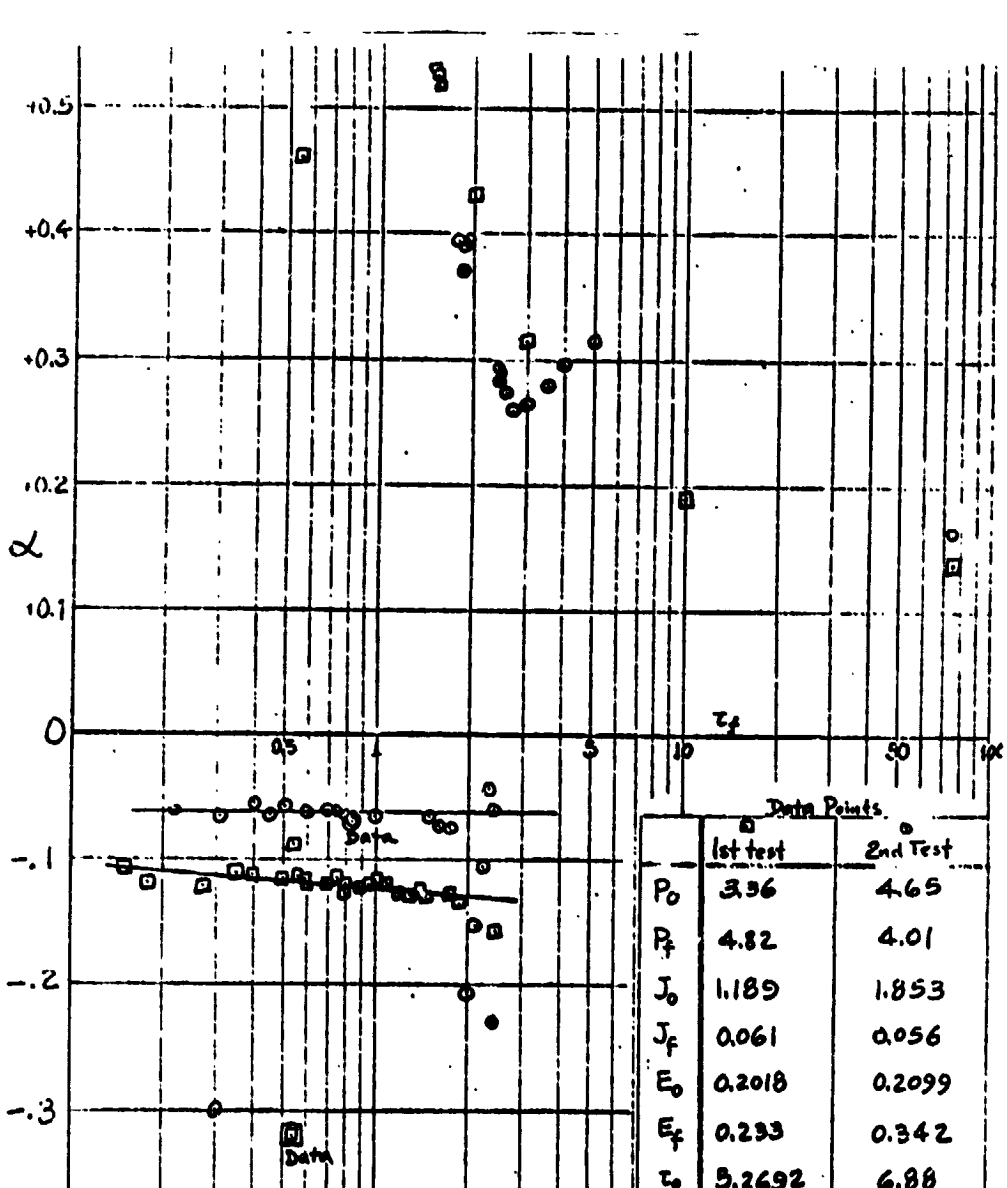

Fig. 1. Survey of α with Different Values of τ_f

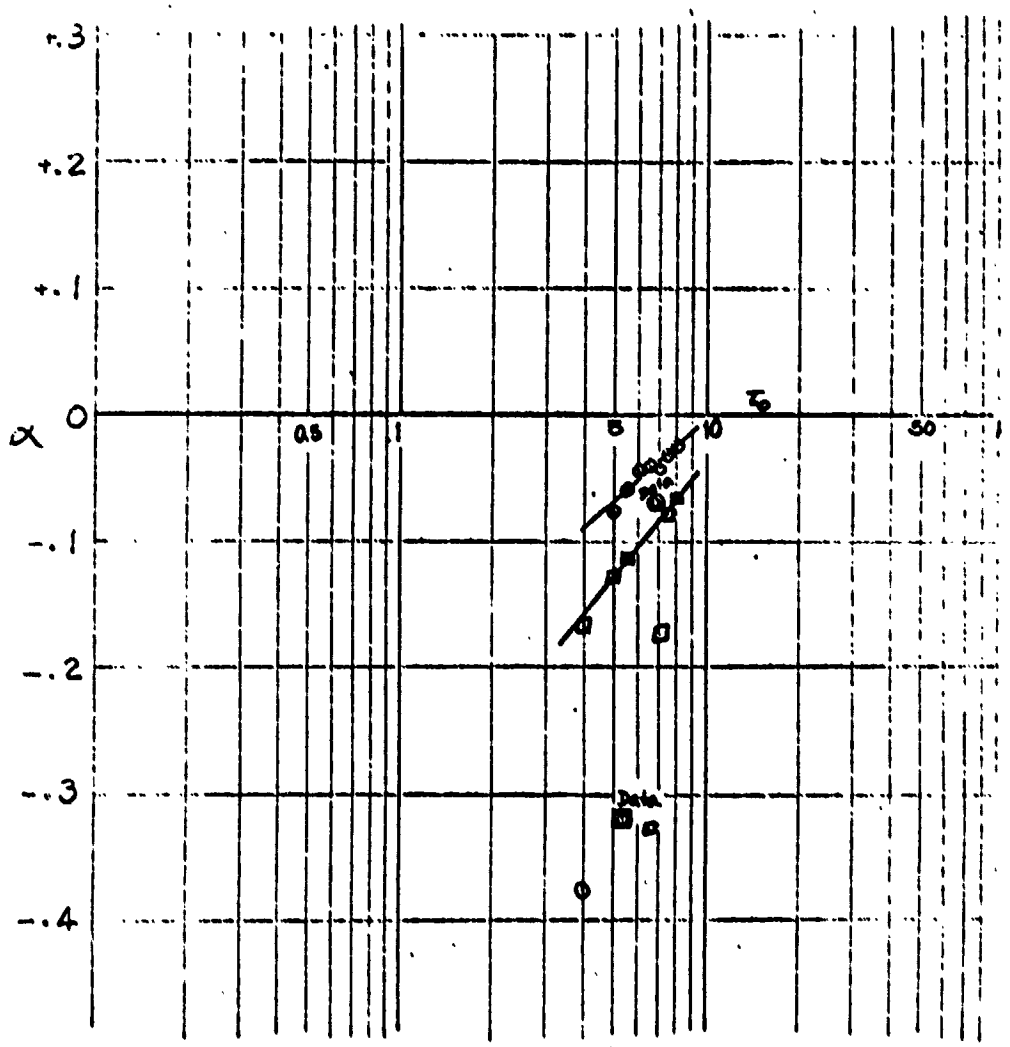

Fig. 11. Survey of α with Different Values of τ_0

APPENDIX C

Computer Programs and Sample Calculations

```
$JOB
C    BIPROPELLANT
C    MARCH 29, 1973
C
C  CURVE 3,FIG.1,PER MARCH 8,DATA FROM RICHMOND
C      SEEKING A PLOT OF LO VERSUS LF
      N=1
      READ(5,100) NCASE
  100 FORMAT(I2)
    1 READ(5,101) RLO,RLF
  101 FORMAT(2F10.6)
      PN=0.
C
      GC=32.2
      THG=0.00026
C
      DPO=62.
      ATO=0.6
      RMO=25.4
C
      DPF=43.3
      ATF=0.945
      RMF=4.30
C
      POO=10.08
      PFF=4.80
      PJO=RLO*RMO/(24.*DPO*ATO*GC*THG)
      PJF=RLF*RMF/(24.*DPF*ATF*GC*THG)
      PEO=0.0721
      PEF=0.241
C
       TO=5.385
       TF=0.5385
C
C   THE FOLLOWING CARDS CONTAIN INFO FOR LATER USE IN VARYING VVO VS VVF
C
C      PCC=1248.
C      VVO=12.5
C      RHOO=0.0411
C      VVF=9.5
C      RHFF=0.0002395
C      RKO=0.01
C      RKF=0.680
C      PEO=RHOO*RKO*VVO/(RMO*THG*(POO+0.5))
C      PFF=RHFF*RKF*VVF/(RMF*THG*(PFF+0.5))
C      POO=5.04    WAS USED IN CURVE 2,FIG.1
C      DPO=124    WAS USED IN CURVE 2, FIG.1
C      DPF=86.6   WAS USED IN CURVE 2,FIG.1
C      PEO=0.1387   WAS USED IN CURVE 2,FIG.1
C       END OF LATENT INFORMATION
C
      AL=0.01
      W=0.01
C
   17 FORMAT(1H1)
      WRITE(6,17)
   18 FORMAT(9X,'LINEAR ENGINE COMBUSTION STABILITY STUDY',/)
      WRITE(6,18)
   20 FORMAT(10X,'LO=',E10.4,5X,'LF=',E10.4,/)
      WRITE(6,20) RLO,RLF
```

```
      19    FORMAT(15X,'ALPHA',11X,'ALPHA 1',15X,'OMEGA',10X,'OMEGA 1',/)
            WRITE(6,19)
    5       ETA=1.
            EVOA=EXP(-TO*AL)
            EVFA=EXP(-TF*AL)
            PPCO=COS(TO*W)
            PPSO=SIN(TO*W)
            PPCF=COS(TF*W)
            PPSF=SIN(TF*W)
            PPCT=1.
            PPST=0.
            AAWW=AL*AL-W*W
      C
            PG=1.+PJO*AL+PJO*PEO*AAWW
            PH=1.+PJF*AL+PJF*PEF*AAWW
            PK=PJO*W*(1.+2.*PEO*AL)
            PNN=PJF*W*(1.+2.*PEF*AL)
            PM=PG-PJO*AL
            PR=PH-PJF*AL
            PU=2.*PJO*PEO*AL*W
            PV=2.*PJF*PEF*AL*W
            PA=AL+1.-PN+PN*ETA*PPCT
            PB=W-PN*ETA*PPST
            CC=EVOA*PPCO
            EE=EVOA*PPSO
            DD=EVFA*PPCF
            FF=EVFA*PPSF
            AJ1=PG*PH-PNN*PK
            AJ2=PH*PK+PNN*PG
            AJ5=PM*PH-PU*PNN
            AJ7=PM*PNN+PH*PU
            AJ9=PR*PG-PK*PV
            AJ11=PR*PK+PG*PV
            PGA=PJO*(1.+2.*PEO*AL)
            PHA=PJF*(1.+2.*PEF*AL)
            PKA=2.*PJO*PEO*W
            PNA=2.*PJF*PEF*W
            PMA=2.*PJO*PEO*AL
            PRA=2.*PJF*PEF*AL
            PUA=PKA
            PVA=PNA
            PAA=1.
            PBA=0.
            CCA=- TO*EVOA*PPCO
            EEA=- TO*EVOA*PPSO
            DDA=- TF*EVFA*PPCF
            FFA=- TF*EVFA*PPSF
            PGW=-PKA
            PHW=-PNA
            PKW=PGA
            PNW=PHA
            PMW=PGW
            PRW=PHW
            PUW=PMA
            PVW=PRA
            PAW=-PBA
            PBW=PAA
            CCW=FFA
            EEW=-CCA
            DDW=FFA
```

```
      FFW=-DDA
C
      CK1=PG*PHA+PGA*PH-PNN*PKA-PNA*PK
      CK2=PH*PKW+PHW*PK+PNN*PGW+PNW*PG
      CK3=PG*PHW+PGW*PH-PNN*PKW-PNW*PK
      CK4=PH*PKA+PHA*PK+PNN*PGA+PNA*PG
      CK5=PMA*PH+PM*PHA-PU*PNA-PUA*PNN
      CK6=PMW*PH+PM*PHW-PUW*PNN-PU*PNW
      CK7=PMA*PNN+PM*PNA+PH*PUA+PHA*PU
      CK8=PMW*PNN+PM*PNW+PHW*PU+PH*PUW
      CK9=PRA*PG+PR*PGA-PKA*PV-PK*PVA
      CK10=PRW*PG+PR*PGW-PKW*PV-PK*PVW
      CK11=PRA*PK+PR*PKA+PGA*PV+PG*PVA
      CK12=PRW*PK+PR*PKW+PGW*PV+PG*PVW
      EEE=PA*AJ1-PB*AJ2+PDD*(CC*AJ5+EE*AJ7)+PFF*(DD*AJ9+FF*AJ11)
      GGG=PB*AJ1+PA*AJ2+PDD*(CC*AJ7-EE*AJ5)+PFF*(DD*AJ11-FF*AJ9)
      EEEA=PAA*AJ1+PA*CK1-PBA*AJ2-PB*CK4
     1    +PDD*(CCA*AJ5+CC*CK5+EEA*AJ7+EE*CK7)
     1    +PFF*(DDA*AJ9+DD*CK9+FFA*AJ11+FF*CK11)
C   END OF EEEA
C
      EEEW=PAW*AJ1+PA*CK3-PBW*AJ2-PB*CK2
     1    +PDD*(CCW*AJ5+CC*CK6+EEW*AJ7+EE*CK8)
     1    +PFF*(DDW*AJ9+DD*CK10+FFW*AJ11+FF*CK12)
C   END OF EEEW
C
      GGGA=PBA*AJ1+PB*CK1+PAA*AJ2+PA*CK4
     1    +PDD*(CCA*AJ7+CC*CK7-EEA*AJ5-EE*CK5)
     1    +PFF*(DDA*AJ11+DD*CK11-FFA*AJ9-FF*CK9)
C   END OF GGGA
C
      GGGW=PBW*AJ1+PB*CK3+PAW*AJ2+PA*CK2
     1    +PDD*(CCW*AJ7+CC*CK8-EEW*AJ5-EE*CK6)
     1    +PFF*(DDW*AJ11+DD*CK12-FFW*AJ9-FF*CK10)
C   END OF GGGW
C
      DFG=EEEA*GGGW-GGGA*EEEW
      GGG1=(GG   EEE-EEEW*GGG)/DFG
      A1=AL-GG
      GGG2=(-G .GA*EEE+EEEA*GGG)/DFG
      W1=W-GGG2
C
   16 FORMAT(10X,2E16.8,5X,2E16.8)
      WRITE(6,16) AL,A1,W,W1
      IF(ABS(GGG1).LT.(0.001).AND.ABS(GGG2).LT.(0.0011)) GO TO 50
      AL=A1
      W=W1
      GO TO 6
   50 IF(NCASE-N)52,52,51
   51 N=N+1
      GO TO 1
   52 WRITE (6,17)
      STOP
      END

$ENTRY
```

LINEAR ENGINE COMBUSTION STABILITY STUDY

L=0.1000E 01 LF=0.5000E 00

ALPHA	ALPHA 1	OMEGA	OMEGA 1
0.10000000E-01	0.51556450E 00	0.10000000E-01	0.41743270E-01
0.51556450E 00	-0.49484670E 00	0.41743270E-01	0.69839530E-01
-0.49484670E 00	-0.30994270E 00	0.69839530E-01	0.72969730E-01
-0.30994270E 00	-0.10960670E 00	0.72969730E-01	0.85579990E-01
-0.10960670E 00	0.15632870E 00	0.85579990E-01	0.15707180E 00
0.15632870E 00	0.89899940E-01	0.15707180E 00	0.86538460E 00
0.89899940E-01	0.49778040E 00	0.86538460E 00	0.37635260E 00
0.49778040E 00	-0.27112540E 00	0.37635260E 00	0.31035610E 00
-0.27112540E 00	-0.11232140E 00	0.31035610E 00	0.33325400E 00
-0.11232140E 00	-0.78895090E-02	0.33325400E 00	0.39047810E 00
-0.78895090E-02	-0.11811030E-03	0.39047810E 00	0.43621950E 00
-0.11811030E-03	-0.47754940E-02	0.43621950E 00	0.43635740E 00
-0.47754940E-02	-0.47305670E-02	0.43635740E 00	0.43636080E 00

```
      $JOB
C     BIPROPELLANT
C       THIS IS CURVE 2, FIG. 4, PER DATA FROM RICHMOND ON MARCH 8,1973
C      SEEKING A PLOT OF VO VERSUS VF
      N=1
      READ(5,100) NCASE
  100 FORMAT(I2)
    1 READ(5,101) VVO,VVF
  101 FORMAT(2F10.4)
      PN=0.
      GC=32.2
      THG=0.00026
      ATO=0.6
      ATF=0.945
      RKO=0.01
      RKF=0.680
      RMO=25.4
      RMF=4.30
      RHOO=0.0411
      RHFF=0.0002385
      DPO=124.
      DPF=86.6
      POO=3.36
      PFF=7.21
      PJO=1.189
      PJF=0.747
      PEO=RHOO*RKO*VVO/(RMO*THG*(POO+0.5))
      PEF=RHFF*RKF*VVF/(RMF*THG*(PFF+0.5))
      TO=5.385
      TF=0.5385
      AL=0.01
      W=0.01
   17 FORMAT(1H1)
      WRITE(6,17)
   18 FORMAT(9X,'LINEAR ENGINE COMBUSTION STABILITY STUDY',/)
      WRITE(6,18)
   20 FORMAT(10X,'VO=',E10.4,5X,'VF=',F10.4,/)
C VO AND VF ARE THE OXIDIZER AND FUEL CAVITY VOLUMES, RESPECTIVELY
      WRITE(6,20) VVO,VVF
   19 FORMAT(15X,'ALPHA',11X,'ALPHA 1',15X,'OMEGA',10X,'OMEGA 1',/)
      WRITE(6,19)
    5 CTA=1.
      EVOA=EXP(-TO*AL)
      EVFA=EXP(-TF*AL)
      PPCO=COS(TO*W)
      PPSO=SIN(TO*W)
      PPCF=COS(TF*W)
      PPSF=SIN(TF*W)
      PPCT=1.
      PPST=0.
      AAWW=AL*AL-W*W
      PG=1.+PJO*AL+PJO*PEO*AAWW
      PH=1.+PJF*AL+PJF*PEF*AAWW
      PK=PJO*W*(1.+2.*PEO*AL)
      PNN=PJF*W*(1.+2.*PEF*AL)
      PM=PG-PJO*AL
      PR=PH-PJF*AL
      PU=2.*PJO*PEO*AL*W
      PV=2.*PJF*PEF*AL*W
      PA=AL+1.-PN+PN*CTA*PPCT
```

```
      PB=W-PN*ETA*PPST
      CC=EVDA*PPCD
      EE=EVDA*PPSD
      DD=EVFA*PPCF
      FF=EVFA*PPSF
      AJ1=PG*PH-PNN*PK
      AJ2=PH*PK+PNN*PG
      AJ5=PM*PH-PU*PNN
      AJ7=PM*PNN+PH*PU
      AJ9=PR*PG-PK*PV
      AJ11=PR*PK+PG*PV
      PGA=PJF*(1.+2.*PEF*AL)
      PHA=PJF*(1.+2.*PLF*AL)
      PKA=2.*PJF*PEF*W
      PNA=2.*PJF*PEF*W
      PMA=2.*PJF*PEF*AL
      PRA=2.*PJF*PEF*AL
      PUA=PKA
      PVA=PNA
      PAA=1.
      PBA=0.
      CCA=-  TF*EVDA*PPCD
      EEA=-  TF*EVDA*PPSD
      DDA=-  TF*EVFA*PPCF
      FFA=-  TF*EVFA*PPSF
      PGW=-PKA
      PHW=-PNA
      PKW=PGA
      PNW=PHA
      PMW=PGW
      PRW=PHW
      PUW=PMA
      PVW=PRA
      PAW=-PBA
      PBW=PAA
      CCW=EEA
      EEW=-CCA
      DDW=FFA
      FFW=-DDA
      CK1=PG*PHA+PGA*PH-PNN*PKA-PNA*PK
      CK2=PH*PKW+PHW*PK+PNN*PGW+PNW*PG
      CK3=PG*PHW+PGW*PH-PNN*PKW-PNW*PK
      CK4=PH*PKA+PHA*PK+PNN*PGA+PNA*PG
      CK5=PMA*PH+PM*PHA-PU*PNA-PUA*PNN
      CK6=PMW*PH+PM*PHW-PUW*PNN-PU*PNW
      CK7=PMA*PNN+PM*PNA+PH*PUA+PHA*PU
      CK8=PMW*PNN+PM*PNW+PHW*PU+PH*PUW
      CK9=PRA*PG+PR*PGA-PKA*PV-PK*PVA
      CK10=PRW*PG+PR*PGW-PKW*PV-PK*PVW
      CK11=PRA*PK+PR*PKA+PGA*PV+PG*PVA
      CK12=PRW*PK+PR*PKW+PGW*PV+PG*PVW
      FFF=PA*AJ1-PH*AJ2+PDD*(CC*AJ5+EE*AJ7)+PFF*(DD*AJ9+FF*AJ11)
      GGG=PH*AJ1+PA*AJ2+PDD*(CC*AJ7-EE*AJ5)+PFF*(DD*AJ11-FF*AJ9)
      FFFA=PAA*AJ1+PA*CK1-PBA*AJ2-PB*CK
     1    +PDD*(CCA*AJ5+CC*CK5+EEA*AJ7+EE*CK7)
     1    +PFF*(DDA*AJ9+DD*CK9+FFA*AJ11+FF*CK11)
      FFFW=PAW*AJ1+PA*CK3-PBW*AJ2-PB*CK2
     1    +PDD*(CCW*AJ5+CC*CK6+EFW*AJ7+FE*CK8)
     1    +PFF*(DDW*AJ9+DD*CK10+FFW*AJ11+FF*CK12)
      GGGA=PBA*AJ1+PB*CK1+PAA*AJ2+PA*CK4
```

```
     1    +P.D)*(CCA*AJ7+CC*CK7-EEA*AJ5-EE*CK5)
     1    +PFF*(DDA*AJ11+DD*CK11-FFA*AJ9-FF*CK9)
112   GGGW=PHW*AJ1+PH*CK3+PAW*AJ2+PA*CK2
     1    +P )D*(CCW*AJ7+CC*CK7-EFW*AJ5-EE*CK6)
     1    +PFF*(DDW*AJ11+DD*CK12-FFW*AJ9-FF*CK10)
113   DFG=EFFA*GGGW-GGGA*EFFW
114   GGG1=(GGGW*FFF-FFFW*GGG)/DFG
115   A1=AL-GGG1
116   GGG2=(-GGGA*FFF+FFFA*GGG)/DFG
117   W1=W-GGG2
118 16    FORMAT(10X,2E16.9,5X,2E16.9)
119   WRITE(6,16) AL,A1,W,W1
120   IF(ABS(GGG1).LT.(0.001).AND.ABS(GGG2).LT.(0.001)) GO TO 50
121   AL=A1
122   W=W1
123   GO TO 5
124 50    IF(NCASE-N)52,52,51
125 51    N=N+1
126   GO TO 1
127 52    WRITE (6,17)
128   STOP
129   END

$ENTRY
```

LINEAR ENGINE COMBUSTION STABILITY STUDY

VI=0.1000E 01 VF=0.3500E 00

ALPHA	ALPHA 1	OMEGA	OMEGA 1
0.10000000E-01	0.15797320E 01	0.10000000E-01	0.14378730E 00
0.15797320E 01	0.14339360E 00	0.14378730E 00	0.15136250E 00
0.18144060E 00	-0.81630980E 00	0.15136250E 00	0.19983600E 01
-0.81630980E 00	-0.63595910E 00	0.19983600E 01	0.19831320E 01
-0.63595910E 00	-0.46504470E 00	0.19831320E 01	0.19674070E 01
-0.46504470E 00	-0.31178210E 00	0.19674070E 01	0.19521880E 01
-0.31178210E 00	-0.19292460E 00	0.19521880E 01	0.19349530E 01
-0.19292460E 00	-0.12670480E 00	0.19349530E 01	0.19151100E 01
-0.12670480E 00	-0.11112710E 00	0.19151100E 01	0.19026530E 01
-0.11112710E 00	-0.11098980E 00	0.19026530E 01	0.19012750E 01
-0.11098980E 00	-0.11099590E 00	0.19012750E 01	0.19012740E 01